AN ABSTRACT OF THE THESIS OF

Paul M. Weitzman for the degree of Master of Science in Mechanical Engineering presented on June 1, 2017.

Title: Practical Application of the Finite Element Method for Vehicle System Loads Analysis.

Abstract approved:

_____

Robert K. Paasch

This work develops the loads, boundary conditions, and model construction techniques used to create a high-level vehicle analysis model. The loads are derived from the overall performance parameters of the vehicle, which include 3 axis accelerations and aerodynamic forces from Computational Fluid Dynamics outputs. The boundary condition of the analysis is the mass of the vehicle directly. The analysis focuses on the vehicle on track, during quasi steady state events such as cornering, acceleration, and braking. The quasi steady state nature of these events is replicated in a linear elastic analysis by using the method of inertia relief. Additionally, a variety of vehicle stiffness parameters including torsional frame, camber, and toe stiffness are measured with the same analysis methodology. Finally, the analysis results are compared to physical testing.

Practical Application of the Finite Element Method for Vehicle System Loads Analysis

by
Paul M. Weitzman

A THESIS

Submitted to

Oregon State University

In partial fulfillment of
the requirements for the
degree of

Master of Science

Presented June 1, 2017
Commencement June 2017

Master of Science thesis of Paul M. Weitzman presented on June 1, 2017

APPROVED:

Major Professor, representing Mechanical Engineering

Head of the school of Mechanical, Industrial, and Manufacturing Engineering

Dean of the Graduate School

I understand that my thesis will become part of the permanent collection of Oregon State University libraries. My signature below authorizes release of my thesis to any reader upon request.

Paul M. Weitzman, Author

ACKNOWLEDGEMENTS

The author would like to thank all current and past members of Global Formula Racing, as the success of the team is the sum of every individual contribution. Specifically, the author would like to thank the chassis sub team for their endless support of composite design and manufacturing.

The author would also like to thank Dr. Paasch for the opportunity to research this topic. The work presented here is only a slice of the knowledge and experience gained being a part of GFR.

Additionally, the following people contributed data to this thesis through the course of their own work on GFR.

Navi Singh provided wing element pressure plots for GFR15c, which were critical in developing accurate aerodynamic load inputs.

Gabe Gray and Sam Conklin set the foundation for using the FEMAP analysis package on GFR.

The GFR15 chassis team provided the sandwich panel test data in Appendix F.

The GFR17 chassis team provided test data for wheel and tire stiffness in Appendix E.

TABLE OF CONTENTS

TABLE OF CONTENTS (Continued)

Page

LIST OF FIGURES

Figure Page

LIST OF FIGURES (Continued)

Figure Page

LIST OF FIGURES (Continued)

Figure Page

LIST OF TABLES

LIST OF TABLES (Continued)

Table Page

LIST OF APPENDICES

PRACTICAL APPLICATION OF THE FINITE ELEMENT METHOD FOR VEHICLE SYSTEM LOADS ANALYSIS

1 INTRODUCTION

The focus of this work is to use Finite Element Analysis (FEA) as a tool to investigate vehicle structural design holistically. The two most important parts of designing a complex, mechanical system are proper identification of the load inputs, and ensuring these loads are analyzed with realistic boundary conditions. Without proper load and boundary condition identification, the functional requirements of the system cannot be met. The purpose of this thesis is developing the loads, boundary conditions, and model construction techniques used to create a structural analysis model of a Formula SAE vehicle.

The approach taken herein is to use the analysis method of inertia relief with a linear elastic model comprised of 1D and 2D elements. Instead of applying constraints directly to a mesh to be analyzed, inertia relief works by applying a reaction force at each grid

point, scaled corresponding to mass, which results in net zero acceleration of the rigid body [1]. Loads are applied identically to a linear elastic model with fixed constraints. Such a model is useful for evaluating the quality of detailed, breakout analysis where the boundary conditions and loads may not be intuitive. Additionally, vehicle stiffness parameters such as hub to hub torsional, toe, and camber stiffness can be evaluated.

The loads on the vehicle are understood as static, dynamic, and aerodynamic forces. Static forces would include the car sitting on the ground at rest, or internal loads such as the driver pressing on the brake pedal. Dynamic forces include acceleration, deceleration, and cornering forces, and data for these forces exist as overall vehicle accelerations. Aerodynamic forces come from the vehicles wing elements, with analysis coming from CFD [2]. These forces are inputs to the analysis presented here, with a simplified vehicle dynamics approach used to determine individual tire forces from these overall accelerations. The Finite Element Model (FEM) presented is simplified from reality through the use of 1D and 2D elements. The boundary conditions on the vehicle exist in the form of mass distribution and different element configurations depending on loading scenario. The output is the load distribution through the vehicle and vehicle stiffness properties.

The model is setup in such a manner to allow the response to be verified with existing data, and to allow extraction of loads to allow designers to properly design parts. Vehicle components could be designed directly within the model, but with the addition of 3D solid elements the analysis run-time can quickly become excessive. Model organization allows new designs to be incorporated, to allow iteration and refinement of loads/parts.

2 BACKGROUND

2.1 Global Formula Racing

Global Formula Racing (GFR) is the partnership of students at Oregon State University and the Duale Hochschule Ravensburg, Badem-Wurttemberg, who come together to design and build two race cars each year to compete in the Formula SAE racing series.

Global Formula Racing first competed for the 2010 FSAE season with 2 combustion powered cars, and since then has designed an electric car in parallel with a combustion car each competition season. The 2015 combustion car used in this thesis can be seen in Figure 1: GFR15c, below.

FIGURE 1: GFR15C (PHOTO CREDIT: ROBERT STORY)

Since 2010 GFR has accumulated 16 overall wins at Formula SAE events, ranging from Formula SAE Michigan (FSAE-M), Formula Student Germany (FSG), and others. Competitions are scored on 1000 points total, and are broken down into different scored areas, with static and dynamics portions, and individual events in each category. The point breakdown is show in Table 1: Competition Points.

Category	FSAE-M	FSG
Presentation	75	75
Engineering Design	150	150
Cost Analysis	100	100
Acceleration	75	75
Skid-Pad	50	75
Autocross	150	100
Efficiency	100	100
Endurance	300	325

TABLE 1: COMPETITION POINTS

Every year, the team goal of GFR is to win every competition entered. This is done by focusing team efforts on areas to which points are most sensitive, which is analyzed by a basic lap time simulation. Areas of the car that are designed this way include things like overall mass, downforce, and horsepower. The structural design of the car stems from the design philosophy of 'simplicity, reliability, and simulation validated by physical testing'. The concept that results from that philosophy is a small, lightweight, single cylinder car, which since 2011 includes an aerodynamic package including wings and an undertray.

Next, we define overall performance parameters that constrain the structural design for the car. These are defined in terms of overall parameters such as lateral acceleration, horsepower, and downforce targets based on the allowable size of the aero package. These requirements are based on mix of lap time simulations and on track data, and are shown in Table 2: Performance Targets. These design goals directly define the structural design requirements of the car.

Name	Value	Description
Steady State Cornering	2.5g	Maximum expected lateral acceleration
Braking	2g	Maximum expected deceleration
Engine Braking	1g	Braking component from engine deceleration
Acceleration	1g	Maximum forward acceleration capability
Bump	3g	Largest expected bump in track
Brake Pedal Force	500 lbs	Maximum force applied at the brake pedal
Downforce @ 80 MPH	556 lbs	Estimated downforce at maximum speed
95^{th} Percentile Driver	220 lbs	Anthropometric Reference Data [3]
5^{th} Percentile Driver	110 lbs	Anthropometric Reference Data [3]

TABLE 2: PERFORMANCE TARGETS

2.1.1 METALLIC STRUCTURES ON GFR

Global Formula Racing makes use of metallic structures in many places, such as the pedal assembly, suspension links, spindle, and suspension clevises. Metallic structures lend themselves well to small volume production environments, particularly the environment the typical Formula SAE team is engaged in which includes the need for rapid design/production turnaround. Designing parts to be machined from monolithic blocks of material allows the engineer several freedoms over composite parts which include ease of structural analysis, no separate tooling required other than hold down fixturing, and good estimations of mass and strength.

FIGURE 2: SPINDLE AND TRIPOD INSERT (PHOTO CREDIT JAY SWIFT)

The design process for metallic structures on GFR typically includes the following. First, the part to be analyzed has the approximate loads derived from component level Free Body Diagrams (FBD). The inputs to FBDs filter back to vehicle performance parameters, namely overall weight of the car, and expected cornering, braking, or acceleration performance, depending on the part and load case analyzed. A part such as a suspension clevis, would then be designed and analyzed using 3D engineering tools. A suspension clevis finite element analysis (FEA) can be seen in Figure 3 below.

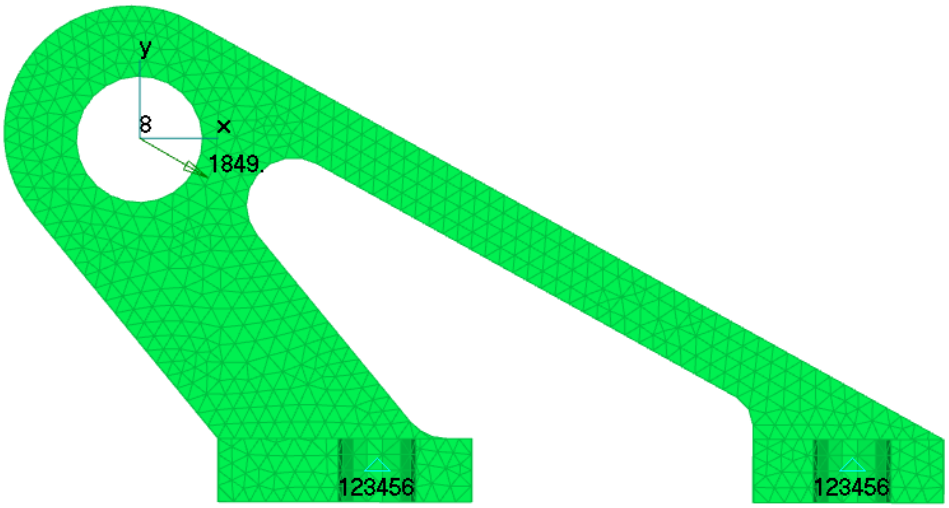

FIGURE 3: LOADS, CONSTRAINS, AND MESH FOR SUSPENSION CLEVIS

Metallic parts are analyzed with some combination of classical hand calculations and finite element analysis. Components such as suspension links are often idealized as two force members with even smaller sub-analysis done on their components. For instance, the tube section of a suspension link may be sized for buckling with hand calculations, while the end that houses the spherical bearing insert may be sized with a 3D FEA using local loads and constraints. A component such as a suspension clevis, however, may be sized solely with FEA. Boundary conditions usually come from rough approximations of reality. For the suspension clevis, fixed constraints are often used because of the high in-plane stiffness connecting the two mounting bolts. In nearly every metallic component on the car, the failure mode at the focus of the analysis is either Von Mises stress or Euler buckling.

2.1.2 COMPOSITE STRUCTURES ON GFR

GFR uses composite materials primarily in the monocoque chassis and aerodynamic components, and several secondary components such as the seat, small brackets, and wheels. The monocoque uses a sandwich construction, with a variety of carbon and core types/thicknesses used. The tooling cost can be substantial for composites so GFR chooses to iterate designs with the specific layup schedules rather than part geometry,

with molds lasting for several seasons. Figure 4 below shows the chassis and general sandwich construction followed.

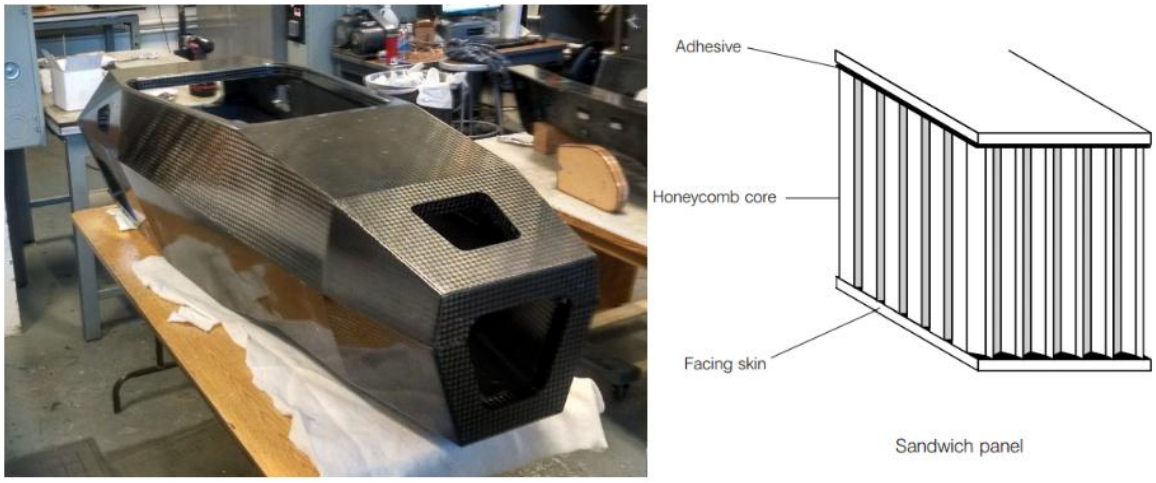

FIGURE 4: MONOCOQUE AND SANDWICH COMPOSITE

The design process for the monocoque chassis begins with vehicle dynamic inputs including torsional stiffness, installed stiffness, toe/camber stiffness, and weight targets, as well as the FSAE Rules. The requirements coming from the rules are summarized in the Table 3 below.

Rule	Name	Requirement
T3.13	Main Hoop Brace Support	Strength and stiffness compared to 2 baseline tubes
T3.14	Front Hoop Bracing	Strength and stiffness compared to 1 baseline tube
T3.18	Front Bulkhead	Strength and stiffness compared to 2 baseline tubes
T3.19	Front Bulkhead Support	Strength and stiffness compared to 3 baseline tubes
T3.24	Side Impact Structure	Energy absorption compared to 3 baseline tubes
T5.4	Shoulder Harness Bar	Strength and stiffness compared to 1 baseline tube

TABLE 3: COMPOSITE CHASSIS FSAE RULES SUMMARY [4]

These requirements are analyzed with beam bending hand calculations to approximate the different regions of the chassis as described in the Rules. These requirements are shown to be met with physical testing. Robert Story created a design tool based on hand calculations that includes analysis of many failure modes and has been shown to be effective at predicting the strength and stiffness of composite panels tested in 3-point bending [5]. Next, the general vehicle requirements such as torsional stiffness and weight

are considered. Due to the complexity of the chassis surface and loading conditions, hand calculations are not used here. A finite element model was developed that allows the simulation of a torsional stiffness test. This simulation includes 2D laminate plates for the chassis, beam elements for roll hoops, and all other components replaced with RBAR elements. The model is shown in Figure 5 below.

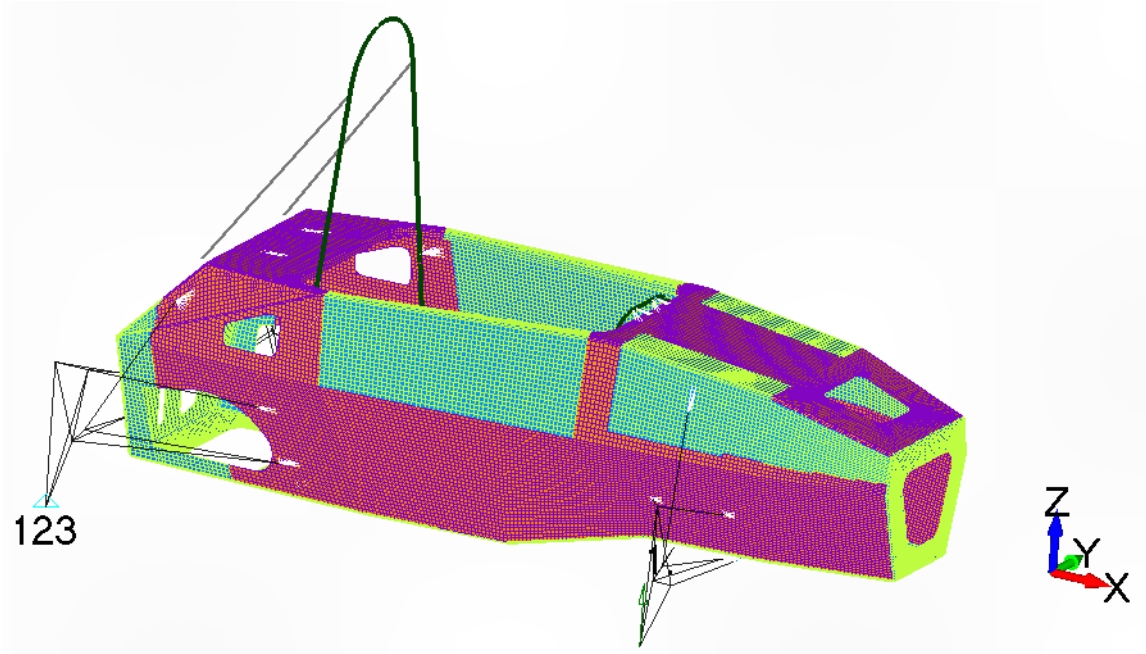

FIGURE 5: SIMPLIFIED CHASSIS ANALYSIS

2.1.3 FASTENED CONNECTIONS ON GFR

Analysis of fastened connections on GFR comes from hand calculations or FEA. As an example, the suspension clevis already introduced is used here. This case is statically indeterminate, so FEA is used to resolve the reaction forces, shown in Table 4. For this case, the clevis has two fixed constraints, and a load of 1849 pounds applied along the shock axis. The reaction forces are used to determine the axial and shear forces required of the mounting bolts. In this case, the X and Y component forces are equal to the Normal and Shear forces at each constraint location. These forces would then be used to size the fasteners at these locations, with the appropriate safety factor.

Reaction Forces			
Component	Bolt 1	Bolt 2	
X	-844.18	-757.06	lbs
Y	499.13	425.38	lbs
Z	0.24	-0.24	lbs
Total	980.69	868.38	lbs

TABLE 4: CLEVIS REACTION FORCES

2.2 Analysis Background

2.2.1 NASTRAN

The space race in the 60s spurred many technological advances. Finite element analysis was a critical part of the design of air and spacecraft in this era, and NASA was a key driver in this [6]. NASTRAN stands for NASA Structural Analysis, and was developed in the 60's, with the first public release was in 1971 and it has been used extensively in industry since being available. In NASTRAN, each type of analysis is handled within a routine called a solution. For this work, we will use NX NASTRAN solution 101, which is linear static analysis. There are many options in NX NASTRAN. A brief description of the primary options utilized in this work are shown in Table 5 below:

	Range	Description
AUTOSPC	0,1	Automatically constrains singularities in the stiffness matrix
GRDPNT	0 or any Grid Point	Grid point weight generator. Option 0 makes the reference the origin of the basic coordinate system. Otherwise, a grid point should be specified. The output is the mass and center of gravity location.
WTMASS	Any Value	This parameter automatically convert weight inputs to mass inputs. To use lbf in a system with inches, it is necessary to convert to slinches.
K6ROT	Any Value	A parameter that gives stiffness to the drilling degree of freedom in CQUAD4 and CTRIA3 elements, to suppress singularities
INREL	0, -1, -2	This is option for engaging inertia relief. Option -1 includes a suport1 entry, Option -2 invokes automatic inertia relief.

TABLE 5: NX NASTRAN OPTIONS [7]

2.2.2 INERTIA RELIEF

Inertia relief is an analysis method developed to analyze unconstrained structures that are in static equilibrium. Typical examples are of an airplane in flight, or a car going around a corner. In the case of an airplane in flight, the body is experiencing lift on the wings, balanced by the force of gravity [1]. In the case of a car going around a corner, the vehicle experiences the force of gravity (reacted at each of the tires) and the force due to the lateral acceleration around the corner.

In a traditional static analysis, the applied loads are reacted at defined points, in a minimum of 6 degrees of freedom. Conversely, when inertia relief is applied, the applied loads are reacted with translational and rotational forces applied to the grid, to force the net acceleration on the body to be zero. These reaction forces are proportional to the system mass. Therefore, one needs to include mass properties, and physical data to properly constrain the system. Additionally, the results from an inertia relief analysis are output with respect to the specified SUPORT1 entry, as there is no absolute ground to the system.

There is published work on the application of the technique in general. Laio shows general 1D, 2D, and 3D implementations for simple structures, and provides multiple simple case studies for understanding the technique [8]. There is also work published on the use of inertia relief for automotive simulations. Anvari and Beigi studied the differences between the inertia relief approach and the transient dynamic approach with a simplified vehicle structure [9]. Their result is that having reasonable accuracy with the inertia relief approach depends on studying load cases that have a driving frequency much less than the natural frequency of the structure. Bryer and Eccles studied the development of vehicle dynamics load cases. They used inertia relief, in combination with segmented load cases as a vehicle approaches steady state cornering, to analyze the body structure [10].

Inertia relief is used with the linear statics solution in Nastran (Sol 101). Boundary conditions in an inertia relief analysis include the SUPORT1 entry and the reference grid

point. The SUPORT1 entry should be selected such that it can restrain all six degrees of freedom in a 3D analysis. It is possible to select multiple grid points, and multiple degrees of freedom, to accomplish this. Loads are applied in an inertia relief analysis in the usual way for a linear statics problem.

2.2.3 ELEMENT TYPES

In this section I will discuss the various element types used in this analysis. I will review how their properties and coordinate systems are defined, and what typical applications these elements have in finite element modeling.

2.2.3.1 Mass elements

To correct the mass of the model for inertial relief constraints, mass elements can be used where it is impractical or unnecessary to use structural elements. The concentrated mass element (CONM2), which describes a mass relative to a grid point, is used in this work. This element allows the definition of a 3x3 symmetric mass moment of inertia to be defined directly, and additionally the mass element center of gravity can be offset from the referenced grid point if necessary. The moment of inertias is by default defined in the basic model coordinate system. The bulk entry format is shown in the can be seen in Appendix B. The property and element definition are one and the same, a mass property card entry directly defines the mass element entry.

2.2.3.2 Spring/Damper Elements

CBUSH elements are 1 dimensional elements that connect 2 grid points. They allow directly defining the stiffness of all 6 degrees of freedom between those grid points, with the appropriate property card. In non-linear analysis, they can additionally define other properties such as general and structural damping. The element coordinate system and bulk entry format can be seen in Appendix A and Appendix B. CBUSH element coordinate systems can be defined either locally, using the element axis and a vector, or globally with a previously defined coordinate system. It is important to note that a CBUSH does not necessarily have zero length, and as such the moment on the element can change based on its length. This is important as it can functionally effect the bending

stiffness of the CBUSH element, and the properties should be developed with this in mind if the analysis is sensitive to such moments.

2.2.3.3 1D Beam Elements

Beam elements are 1 dimensional elements that connect 2 grid points. The beam elements discussed here are CBEAMs. They are described by an appropriate property card, which typically is based on a standard beam cross-section such as a circular rod, rectangular tube, etc. They are used to represent simple cross section parts, things that are either constant or easily described (varying per functions). The coordinate system X axis is defined as the vector between the defining grid points, and the origin is the first grid point. The coordinate system and element bulk entry can be seen in Appendix A and Appendix B. Additionally, beams can be offset along either their Y or Z axis. This is useful for getting the axial load moment correct, by offsetting the beam neutral axis. The property card definition includes the moment of inertia, torsional constant material properties, etc. The general property card can be seen in Appendix C.

The use of beams is ideally suited to a variety of tube and extrusion based structures, especially where the performance at nodes is not of critical importance. These structures could include tube space frames, suspension links, strut members, etc.

2.2.3.4 2D Shell Elements

2D shells are some of the most versatile elements at our disposal. They can be used to represent a wide variety of structures, web and rib metallic structures, shell structures, etc., and have several element definitions as well. For this paper, we will focus on two element types only, CQUAD4 and CTRIA3. These elements are described by 4 and 3 grid points, respectively, and do not have midside nodes. The definitions for both elements are nearly identical, therefore only CQUAD4 will be discussed here. The coordinate system is defined by the first edge and the right-hand rule, see Appendix A for a detailed view. One critical detail about these 2D elements is that it doesn't transfer the moment about its normal axis at its grid points. Therefore, it is possible to have a singular stiffness matrix, or more commonly, strange results where line elements connect to these

grid points directly. The previously mentioned ‘K6ROT’ parameter gives this rotation a base stiffness to eliminate the singularity.

In this work, plate shells will be used to represent isotropic materials only. As such, it is only necessary to define thickness in the T1 direction. In the context of mass sensitive analysis, 2D plate elements have a non-structural mass property. This is mass per unit area that can be added without any structural effect to the element, and is useful for representing paint, adhesives, coatings, etc. that are distributed over the element surface. Layup cards are necessary to define composite laminates. For 2D shells, the layup cards reference the defined material direction. Each layer is defined by a material thickness, and typically an orthotropic material card, for most composite materials such as honeycomb core and carbon face sheets [11]. Laminate shells are primarily defined from the layup card selected. The detailed property card for laminates and plates, and layup card can be seen in Appendix C.

2.2.3.5 Rigid Elements

Rigid type elements come in many forms, but the ones discussed here are RBE2 and RBE3 elements. These types of elements are used in this work primarily in defining connections between different mesh types. These are technically not elements, but multi-point constraints that define a relationship between grid points [12].

RBE2 elements are defined by a single independent node and any number of dependent nodes. The independent node has 6 degrees of freedom, and can enforce up to all 6 DOFs onto its dependent nodes. The RBE2 acts as a rigid constraint, and will add stiffness to the model. Therefore, it is necessary to use these with care. In this work, they are used in two ways. The first is in place of structures that are significantly more rigid than their support structures, such as the engine block. The second is at clevis, where a bolt is missing. The bolt provides significant out of plane stiffness to a double shear clevis, and including an RBE2 in its place is a reasonable approximation that simplifies modeling.

RBE3 elements are also defined by a single independent node and any number of dependent nodes. The independent node supports up to 6 degrees of freedom. The

dependent nodes also support up to 6 degrees of freedom, although it is generally recommended to only enforce translation for this element type. These elements are useful when connecting structures, where all component stiffness's already exist in the model and/or meshes don't line up to facilitate direct connection. As they don't enforce any stiffness in the model, they work more to 'smear' the force between components. In this work, they primarily are used at bolted interfaces, such as suspension clevises to monocoque.

3 METHODOLOGY

In this section I will describe the methods used to derive vehicle level performance and stiffness properties, element level properties, and validate specific model construction methods.

First, I will describe how values for vehicle performance targets are reached. Then, I will review data for the torsional, toe, and camber stiffness of the vehicle. I will additionally gather and review data for suspension link forces, based on cornering forces. Next, I will show how I setup more complicated regions of the vehicle model and explain and validate the specific details of these techniques, including assumptions made and details of element formulations when required. This will include using CBUSHs for all bolted connections, using 2D laminate shells in place of 3D laminates, using 2D isotropic plates to represent aluminum suspension clevis's, and the use of CBUSHs in place of large bearings such as in the differential housing. Finally, I will validate the general method of simulation (inertia relief). I will setup a simple beam bending simulation to validate this, based on gravitational loading.

3.1 Vehicle Properties

In the following section, I will first discuss how the specific values for the various high level vehicle performance targets, and how those are divided into different distinct load cases. Then, I will discuss general vehicle stiffness targets, and how those targets are reached.

3.1.1 PERFORMANCE PROPERTIES

The high-level performance envelope is defined in this section. The design assumptions are first described, and then general validation is shown to verify these assumptions from track conditions. Finally, the general combination of loads used to develop analysis load cases is described. The general design parameters for the vehicle include aerodynamic forces, static forces, and dynamic forces. Static and dynamic loads are initially described by their relative accelerations compared to gravity, for instance, a 2g lateral acceleration would exert a force equal to twice the cars static weight in the Y-axis direction. An example acceleration and cornering free body diagram is shown in Figure 6 below.

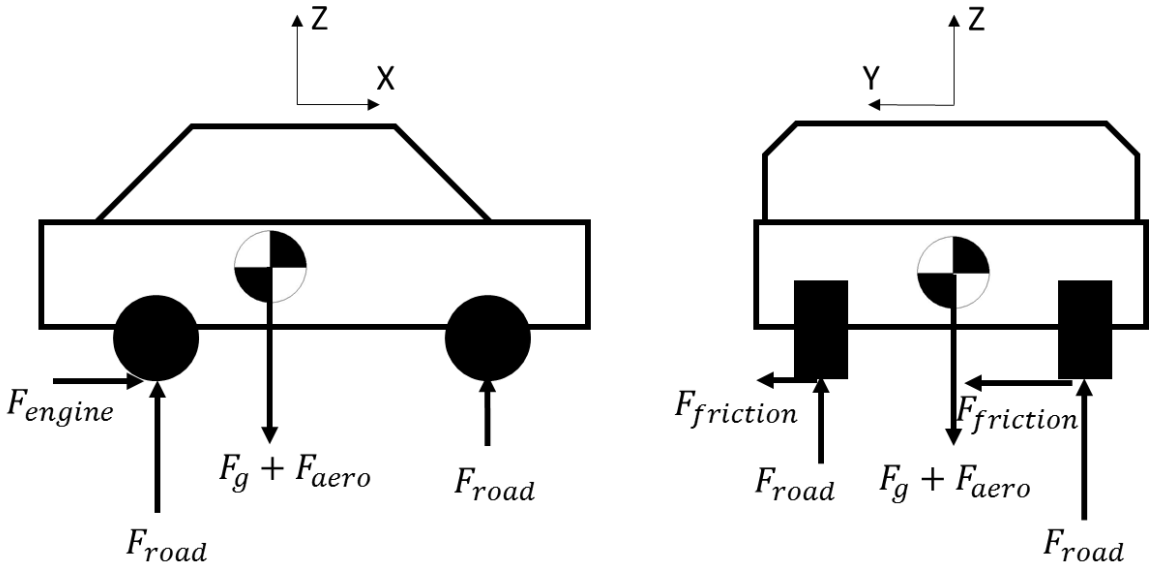

FIGURE 6: ACCELERATION AND CORNERING FBD

Aerodynamic forces are predicted from computational fluid dynamics software, based on the geometry of the vehicle and wings, ride height, yaw angle, and other factors. This is usually evaluated at an average speed of 40 miles per hour. These forces include those acting by pressure on the body and wing elements, as well as the reaction forces at the tires due to those forces. The simplest way to validate these forces is with coast down testing, whereby the additional aerodynamic download on the shocks is measured. This is done elsewhere as it is not the focus of this work. If laminar flow is maintained, the aero download can be expected to follow the velocity squared relationship. The static forces

include the stationary weight of the vehicle and driver. The dynamic forces include those related to the acceleration of the vehicle. The accelerations include normal acceleration, braking deceleration, cornering, and the reaction due to the vehicle hitting a bump. Lateral and longitudinal acceleration data as measured on the vehicle can be found in Figure 7, and highlighted are different load cases to be analyzed. Table 6 below shows all the preceding forces grouped into different driving regimes where they could act on the vehicle at once.

Vehicle Load Case	Aerodynamic Force @ 40 mph	Static Weight	Cornering	Acceleration	Braking	Bump
Acceleration		X		X		
Corner Entry	X	X	X		X	
Steady State Cornering	X	X	X			
Corner Exit	X	X	X	X		
Braking	X	X			X	
Bump	X	X				X

TABLE 6: PERFORMANCE PROPERTIES

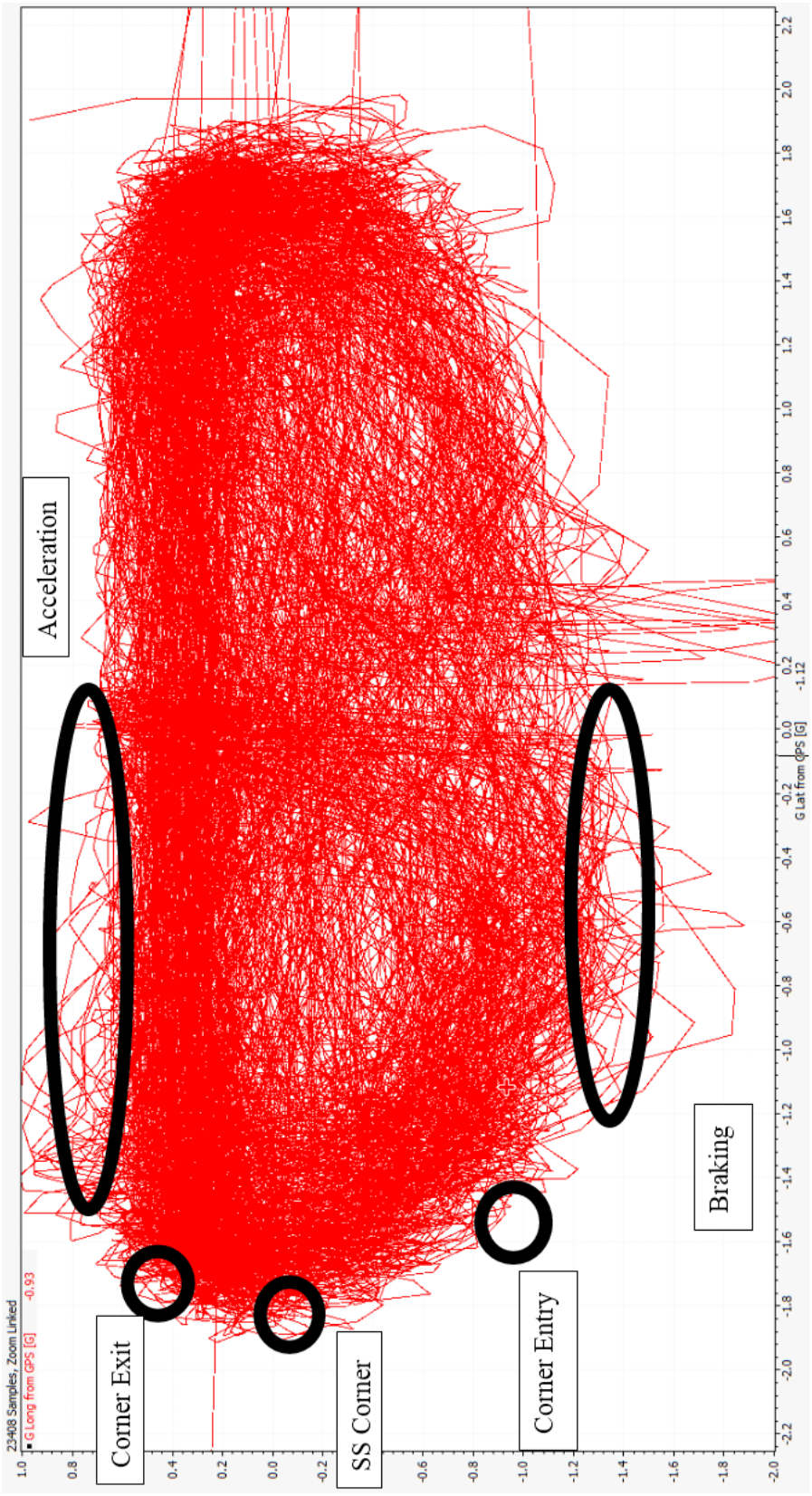

FIGURE 7: LOAD REGIMES

3.1.2 STIFFNESS PROPERTIES

Vehicle stiffness properties define the vehicles relationship to its core vehicle dynamics in addition to the feedback of the car to the driver. The magnitude of the following properties defines the interaction to the tires and spring/damper combination.

The group of properties discussed is related to torsional stiffness. Torsional stiffness is defined as the vehicles response to a twisting moment. There are 3 components looked at here. Hub to hub stiffness is defined as rotational stiffness about the vehicle X-axis, not including the tire or wheel center contribution. Installed stiffness is defined as the stiffness of the outboard suspension and its connection to the frame. It does not include the stiffness contribution from the tire and wheel center. Chassis stiffness is defined as the frame twist stiffness about the X-axis, measured from the front and rear vertical chassis planes. The measurement points lie on the bottom portion of both regions. These 3 properties are determined in a single test, following published work that illustrates this test [13]. This method involves using roller plates, corner scales, and a jack to apply a moment to the suspension in the most unconstrained way possible. The results are shown in Table 7.

The next group of properties relate to the installed suspension package. They include the toe and camber stiffness taken at the front and rear suspension. On the front, the stiffness is measured with steering locks fitted to the steering rack, which restricts steering movement. On the front and rear, the tire and wheel shell are replaced with rigid aluminum plates. The values from these tests are shown below.

	Front	Rear	Total	
Hub to hub			2511	ft-lb/deg
Installed	11409	7475		ft-lb/deg
Frame			5593	ft-lb/deg
Toe	57	141		ft-lb/deg
Camber	293	315		ft-lb/deg

TABLE 7: VEHICLE STIFFNESS PROPERTIES

3.2 Element Properties

The properties chosen for stiffness and mass of the elements is important to any FE model. Without having the correct stiffness one can never hope to have an accurate result. In this section I will describe the properties used for each element type.

3.2.1 Mass Elements

Mass elements are used wherever components that have either difficult to model, or unknown structural properties, but still need their mass accounted for. Mass elements that are of low individual contribution to the vehicle mass (~1-2%) are represented as simple point masses, placed near correct center of gravity location for each, with RBE3s to connect to the surrounding structure to not add stiffness. In some instances, such as paint, adhesive, or rows of fasteners, the 'non-structural mass' property is used to distributed mass through the structure. In Table 8, these unmodeled components are summarized.

Component	Mass (lbs)	Qty	Total (lbs)
Batteries	2.5	2	5
ECU	1.1	1	1.1
ACL	1.5	1	1.5
VIM	0.5	5	2.5
Wiring	5	1	5
Brake System	1	4	4
Master Cylinders	2	1	2
Tank + Fuel	10	1	10
Fasteners	10	1	10
Chain	1	1	1
Intake	3	1	3
Exhaust	10	1	10
Pneumatic system	5	1	5
Total Unmodeled mass			60.1

Table 8: Small Mass Properties

The two largest unmodeled components are the engine and the driver. The engine is represented by a single RBE2 element, as this will appropriately capture the extremely high stiffness of the engine relative to other components. The dependent nodes are at critical interface points such as engine mounts and sprocket. The independent node is

located at the approximate center of gravity of the engine. The driver is represented by a single RBE3 element as this load is well distributed into the floor and sides of the chassis, and the drivers' body is deformable and doesn't add stiffness to the structure. Both components have their approximate moment of inertias calculated.

The engine is measured at 77 pounds, and the moment of inertia is simplified to a homogeneous rectangular block, symmetric about the global ZX plane. The height, *h*, is 15 inches. The width, *w*, is 9 inches. The depth, *d*, is 13 inches. The plan view can be seen in reference to the vehicle in Appendix D. The simplified block's MOI is calculated based on the standard cuboid formulation, shown below.

$$I_{xx} = \frac{m(h^2 + d^2)}{12} = 1530\ lb - in^2$$

$$I_{yy} = \frac{m(w^2 + d^2)}{12} = 1970\ lb - in^2$$

$$I_{zz} = \frac{m(w^2 + h^2)}{12} = 1250\ lb - in^2$$

The heaviest driver used is the 95th percentile male, which is 220 pounds. Actual, and minimum, driver weights are not included in this analysis as they will result is less load in the structure. The driver is separated into 5 homogeneous shapes, with their individual weights approximated, dimensions approximated and the parallel axis theorem applied to get all six MOI's about a grid point. The plan view of these, with the standard dummy, 'Percy', can be seen in Appendix D. The individual contributions are tabulated below in Table 9.

Component	Ixx	Iyy	Izz	
Head	561	722	458	lb-in^2
Upper Body	842	1084	688	lb-in^2
Torso	1964	2528	1604	lb-in^2
Upper Legs	1403	1806	1146	lb-in^2
Lower Legs	842	1084	688	lb-in^2
Total, Translated	61798	7223	27738	lb-in^2

TABLE 9: DRIVER MASS PROPERTIES

3.2.2 CBUSH ELEMENTS

To support analysis of the whole vehicle, the joints must be modeled. For simplicity and speed in the analysis, a single CBUSH element is used to summarize the stiffness of each bolted connection. In this section I will develop the equations used to create a joint stiffness calculator, where the stiffness in each degree of freedom for every bolted joint is estimated.

The first degree of freedom represents the axial stiffness. This is approximated based on the bolt material properties, including the Young's modulus E_f of the bolt, its diameter *d,* and its length, *l*.

$$K_1 = \frac{E_f * \pi * d^2}{4 * l}$$

The second and third degree of freedoms represent the shear stiffness of the joint. There are many existing formulations, with most only applicable to certain joint configurations. The one used here was developed by Huth, and is generally regarded as a conservative approximation [14]. The variables include the Young's modulus of the top and bottom plates, E_1 and E_2, the thickness of the top and bottom plates, t_1 and t_2, and three coefficients, *a*, *b*, and *n*. I am assuming the in-plane properties are identical in the 0 and 90 degree directions, therefore, the 2 and 3 degrees of freedom are identical.

$$K_2 = K_3 = \frac{1}{C}$$

$$C = \left(\frac{t_1 + t_2}{4 * l}\right)^a * \frac{b}{n} * \left(\frac{1}{t_1 E_1} + \frac{1}{n t_2 E_2} + \frac{1}{n t_1 E_3} + \frac{1}{2 n t_2 E_3}\right)$$

The fourth degree of freedom relates to the torsional stiffness of the joint. While this may be a difficult property to estimate, as it related to bolt size, materials, torque preload, and friction, in practice it is not necessary to accurately predict. No proper engineered joint should rely on this stiffness for the joint to function, and as such there are usually at least 2 bolts in a joint, so that this moment is carried in shear in the bolt pair. I have included

an approximation based on the bolt torsional stiffness, *J*, the shear modulus, *G*, and the bolt length *L*.

$$K_4 = \frac{J * G}{L}$$

The fifth and sixth degrees of freedom relate to the bending stiffness of the joint. Knowledge of the bending stiffness of a joint is less important than the axial and shear properties because in practice the bending at a joint is reacted in the substrates, and results in additional tensile force in the joint. However, in practice this contact is not typically modeled, especially in a large model with many contact surfaces as it would needlessly increase simulation time. It is important to have a reasonably large value for these bending stiffness's when contact is not modeled in FEM, so that the additional tensile load can be calculated. A simplified approach is used, where the average substrate stiffness's and total joint thickness is used with a cantilever beam formula. An assumed amount of contact is used, based on the fastener diameter. This approach is only valid for the case where there is no separation between the base materials.

$$K_5 = K_6 = \frac{4 * E * I_x}{h * L^2}$$

3.2.3 Isotropic Plates and beams

All metallic structures are assumed to be isotropic. There are three main materials that fall under this category, Ductile Iron, 4130 Steel, and 6061-T6 Aluminum. The properties come from the MMPDS-01 handbook. Their values are summarized in Table 10 below.

Property	Ductile Iron	4130 Steel	6061-T6 Aluminum	Unit
E	24.0	29.7	10.3	msi
G	9.4	11.5	4.0	msi
Poisson Ratio	0.275	0.290	0.275	-
Density	0.280	0.280	0.098	lbs/in^3

Table 10: Isotropic Material Properties [15]

3.2.4 TIRE PLATE ELEMENTS

The tires are a particularly difficult component to model structurally. There are many unknowns with the quantity and types of reinforcements that make up a radial or bias ply tire that is proprietary information, unavailable for use. Therefore, the approach taken is an empirical one. The specific tires used are mounted on an Instron test machine, and loaded in the road normal direction. These test results can be seen in Appendix E. A subscale finite element model made to replicate this test is created to be able to include air pressure. As there is a large, variable, interface between the load applicator and the tire, contact properties are used, based on the work of [16]. A cross section of the finite element model showing element types and constraints can be seen in Figure 8 below. Corded rubber mechanical properties are based on textbook data [17], and are summarized in Table 11. Air is assumed to behave as an ideal gas with the bulk modulus equal to the pressure. This is approximated by using 3D orthotropic properties, with the E_1, E_2, E_3 modulus equal to the air pressure, and an exceedingly low value for G_{12}, G_{23}, and G_{13}. Then, the load distribution into the wheel center bolts is presented in Figure 10. These results are summarized in Appendix E.

Property	Tire Tread	Tire Body	Tire Bead	Unit
E	3000	800	50000	psi
G	1007	268	19231	psi
Poisson Ratio	0.49	0.49	0.3	

TABLE 11: INITIAL TIRE PROPERTIES

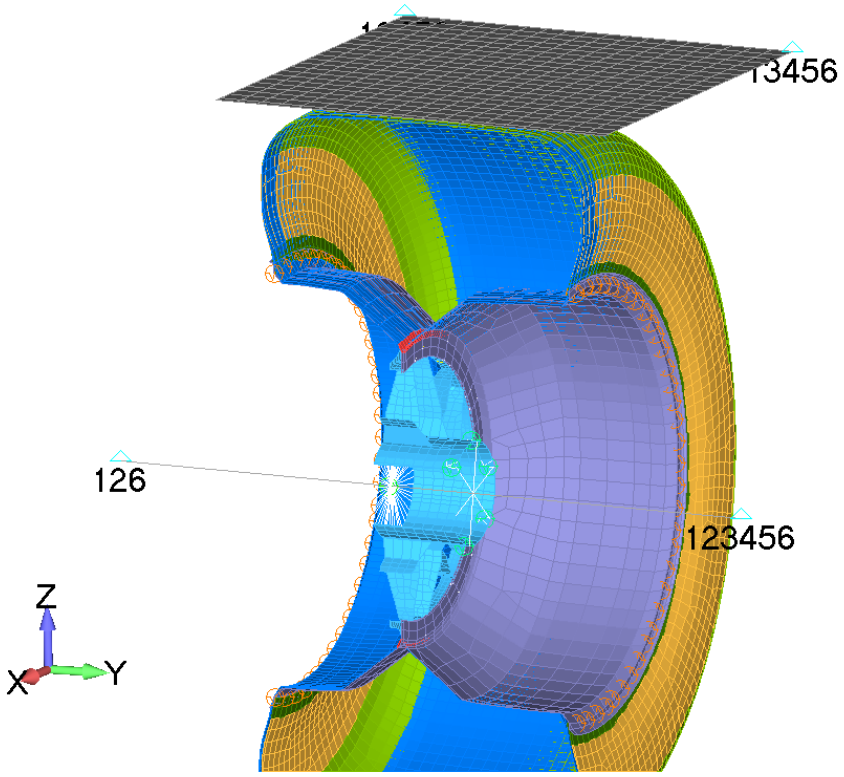

FIGURE 8: TIRE FEM

The primary factor in the stiffness of a tire is seen to be internal air pressure, however, this is impractical to include in the complete vehicle simulation. The breakout tire simulation takes approximately 60 minutes to solve. Therefore, a simplified tire model that excludes air pressure is created. The plate properties are then matched in FEA to give a similar response to a tire pressurized to 22 psi, as this is higher than any expected pressure and will result in a stiffer tire, as shown in Figure 9. The properties used are shown in Table 12 below. The tire to wheel shell connection force comparison between the air filled model and the simplified model is shown in Figure 10 below.

Property	Tire Tread	Tire Body	Tire Bead	Unit
E	25	10	150	ksi
G	25	10	150	ksi
Poisson's Ratio	0.49	0.49	0.49	

TABLE 12: FINAL TIRE PROPERTIES

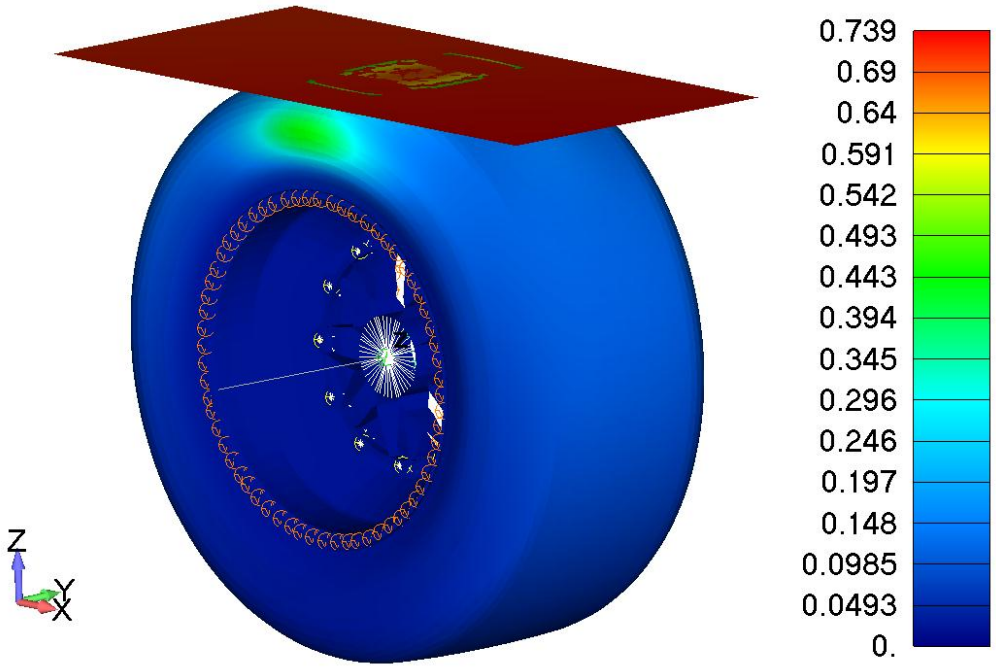

FIGURE 9: TIRE DISPLACEMENT CONTOUR - SIMPLIFIED MODEL

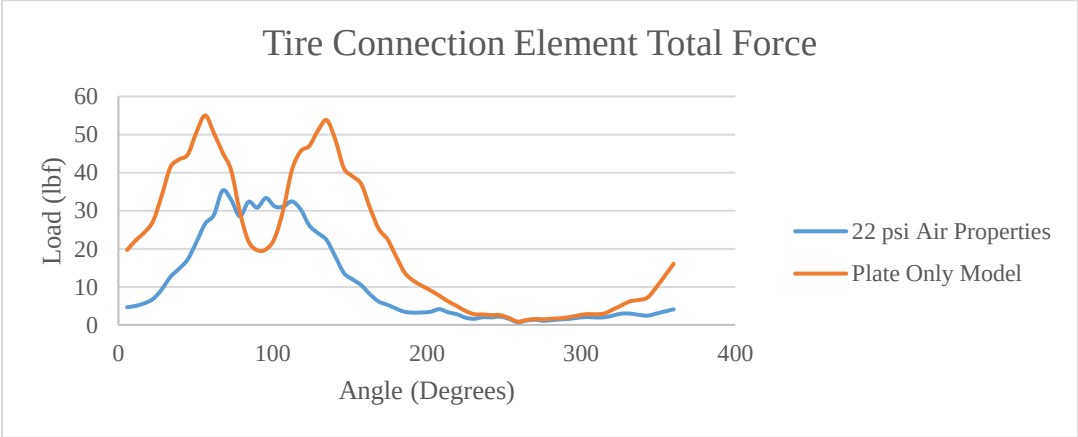

FIGURE 10: INTERFACE FORCE COMPARISON

3.2.5 LAMINATE PLATE ELEMENTS

For proper response of the sandwich structure, it is important to use accurate, real world values for the mechanical properties of the carbon fabric and the honeycomb core layer. Where available, tested values are used to appropriately reflect the manufacturing sensitive nature of composite structures. The three materials discussed here are Toray

T700S-12K-50C/#2510 Plain Weave Fabric (F6273C-07M), Toray M46J-12K-#2510 Unidirectional Fabric, and Hexcel HRH-10-1/8-3.0 Nomex Honeycomb core. The carbon and honeycomb properties with sources are listed in Table 13 below.

Property	T700 Weave	M46J Uni	HRH-10 Core	Unit
E1	8000	38400	0.1	ksi
E2	8000	100	0.1	ksi
G12	610	10	0.1	ksi
G1z	80	320	6	ksi
G2z	80	6.8	3.5	ksi
Poisson Ratio	0.04	0.04	0	-
Density	0.052	0.06	0.0017	lbs/in3
Cured Ply Thickness	0.0085	0.0037	-	in

TABLE 13: COMPOSITE MATERIAL PROPERTIES [18] [19]

There are additional structural materials involved in the sandwich structures used including film adhesive, core splice, and paste adhesives, but they are excluded from this analysis.

3.3 Model Construction Techniques

3.3.1 CBUSH ELEMENTS FOR BOLTED CONNECTIONS

As bolts are the primary mechanism connecting most components on the car, their FEM modeling technique is analyzed in some detail here, with multiple modeling options considered. There are many detailed analytic and FEM approaches are considered in academia, including those that consider the detailed geometry of the bolt [20], which are on the surface not practical to an application with hundreds of fasteners to be analyzed in each run. The modeling alone would be prohibitive, not to mention excessive computation time. The first technique reviewed is from Predictive Engineering, and will be used as a baseline to judge the effectiveness of other approaches [21]. The approach includes the use of bolt preload and linear contact regions at the connection interface to simulate a bolted interface. Bolt preload F_i is based off a standard torque, T, for ¼" bolt, calculations from Shigley's, with 50 ft-lbs of torque. The bolt condition factor K is

chosen based on common factors [22]. The FEM and displacement contour for this approach is seen below in Figure 11.

$$T = KF_i d$$

	Value	Unit
T	25	ft-lb
K	0.2	
d	0.25	in

$$F_i = 500\ lbf$$

Although this is a reasonable approach, it is still too labor and computationally expensive to use this style connection in the full vehicle model. The computation time is approximately 200 seconds. For the vehicle level model, a 2d plate model with a CBUSH connection was considered (Figure 12). The CBUSH element properties are calculated using the approach described in the previous section. See below for a comparison of results between these approaches. The error is 1.5% compared to the Predictive Engineering approach, and the computation time was only seconds.

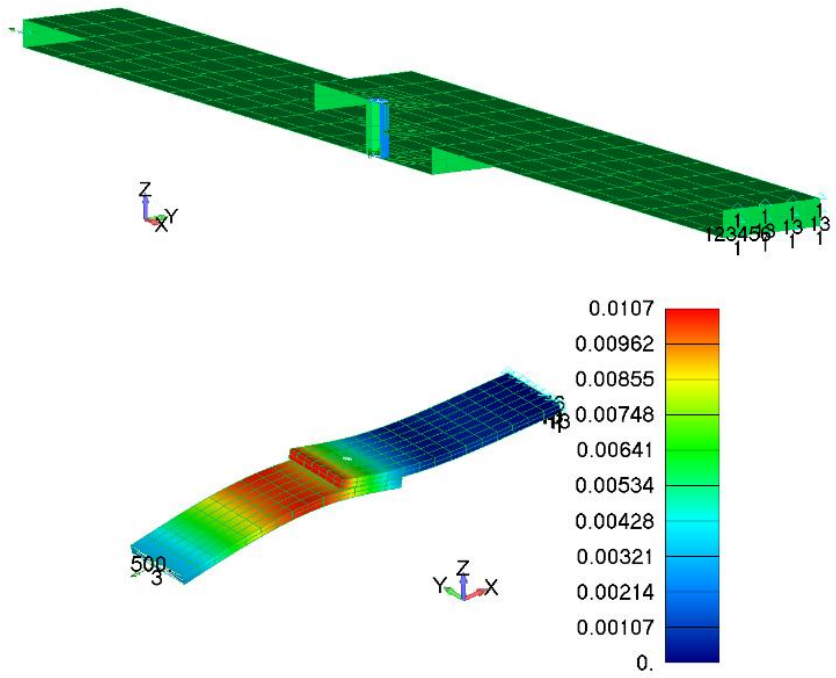

FIGURE 11: BOLTED CONNECTION ANALYSIS, 3D MESH

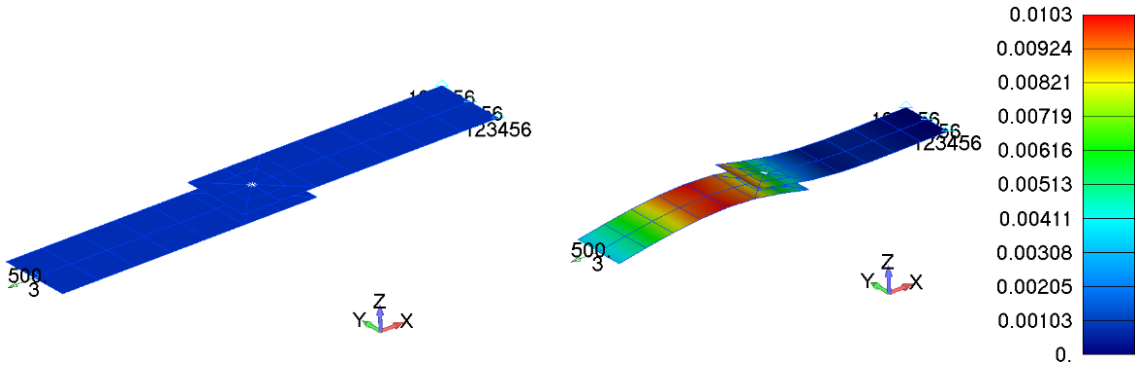

FIGURE 12: BOLTED CONNECTION ANALYSIS, 2D MESH

3.3.2 SANDWICH PANEL

As the main torsional spring in the system, it is important to ensure that the modeling approach used is representative of reality. As such, I will show that a simple 2d laminate plate provides sufficient accuracy. As composite sandwich panels are highly dependent on the manufacturing process, I will compare physical 3-point bend tests to those in FEM. 2D laminates are adequate for general system response, which is the most important part for a full vehicle sim. While the shortcomings are that one cannot evaluate failures through the thickness of the composite, if one is not looking for these specific failure modes then this adequate. Additionally, simulation time is a large shortcoming of 3D FEMs in general, so avoiding these is desirable. GFR has tested many sandwich constructions in 3-point bending tests. The physical test of one sample that relates to the general construction of the chassis, the layup schedule and results are included in Appendix F. The FEA results are shown in Figure 13 below.

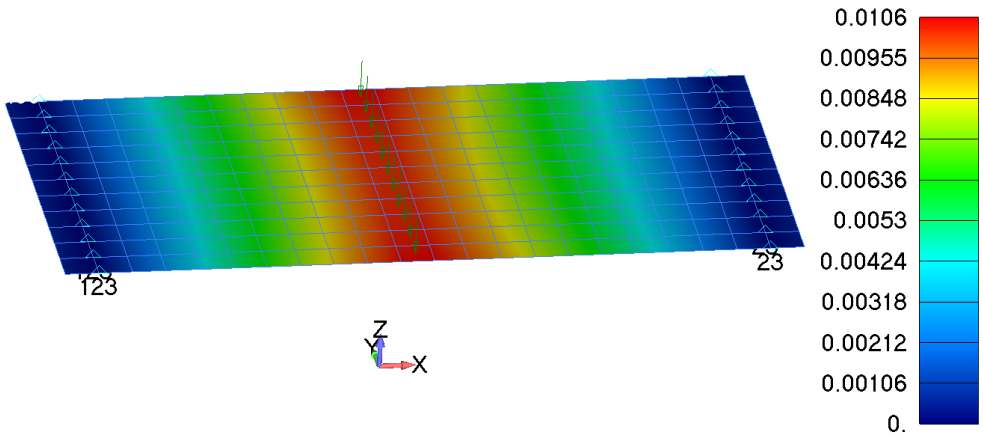

FIGURE 13: COMPOSITE PANEL SIMULATED DEFLECTION

Tested	Gradient	1350	N/mm
	Rig compliance	6266	N/mm
	Stiffness	1720	N/mm
Simulated	Stiffness	1652	N/mm
	Error	3.98	%

TABLE 14: SANDWICH PANEL STIFFNESS

3.3.3 2D PLATE

In this section I will show that it is acceptable to replace 3D components with 2D ones approximated by plate elements. It is essential to do this to manage simulation time in a large model. In this example, I will apply similar loads and constraints to the front shock clevis, and compare the peak Von Mises stress, overall stress gradient, and reaction forces between the 3D and 2D models. The properties described previously for 6061-T6 aluminum are used for this analysis.

The 3D finite element model is meshed using tetrahedral elements, which results in 47,000 elements. The geometry used for meshing is simplified from the as machined geometry, eliminating small chamfers near bushings. The 3D FEA takes approximately 45 seconds to run. The 2D model is meshed using a mixture of hexahedral and tetrahedral elements, which results in 192 elements. The 2D FEA takes a fraction of a second to run. In both cases, the applied loads are distributed through RBE3 elements at the bushing

openings, along the shock vector. The constraints used are fully fixed. The stress contours can be seen in Figure 14. The reaction force comparison can be seen below in Table 15.

Component	3D, Node 1	3D, Node 2	2D, Node 1	2D, Node 2	Error
X	-844.18	-757.06	-852.07	-749.17	0.99%
Y	499.13	425.38	503.83	420.67	1.03%
Z	0.24	-0.24	0.05	-0.05	77.87%
Total	980.69	868.38	989.88	859.19	1.00%

TABLE 15: CLEVIS REACTION FORCES

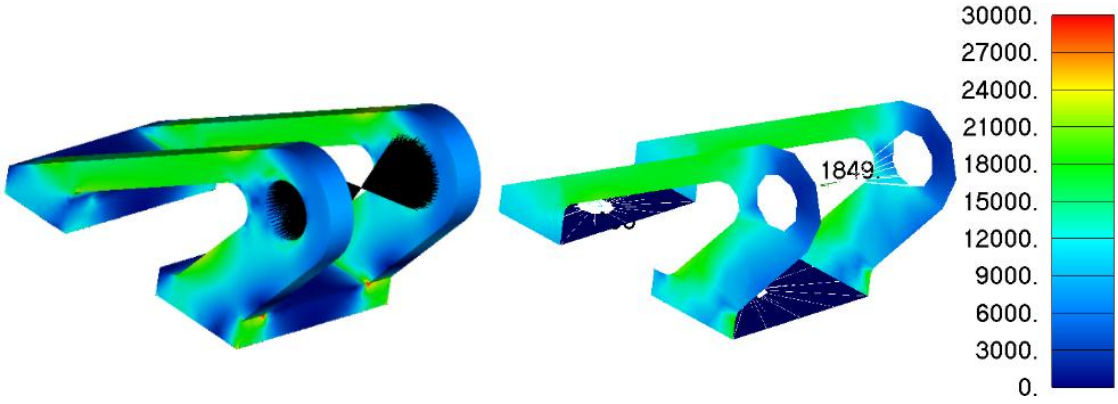

FIGURE 14: SHOCK CLEVIS COMPARISON

3.3.4 CBUSH ELEMENTS FOR BEARING CONNECTIONS

Due to the complexity and computational cost of analyzing contact around bearing interfaces, they must be simplified to keep simulation time down in a full vehicle model. This is because solving for contact results in a geometrically non-linear solution. For small bolted connections, the bearing interface is replaced with an RBE3 element, and as shown previously, this gives reasonable accuracy. For large bearing connections, such as the differential or spindle connections, more investigation into the method is required to ensure sufficient accuracy.

In this section I will use the rear differential to compare a method utilizing CBUSH's around the bearing surface, to one that uses contact (GAP) elements around the bearing. The modeling of both approaches is similar, as the only difference is the replacement of GAP elements with CBUSH elements, and their respective properties. The modeling details can be seen in the following section, and the properties used for this test case are

shown in Table 16 and Table 17. Figure 15 shows a comparison of the resultant forces in the CBUSH and GAP element approach.

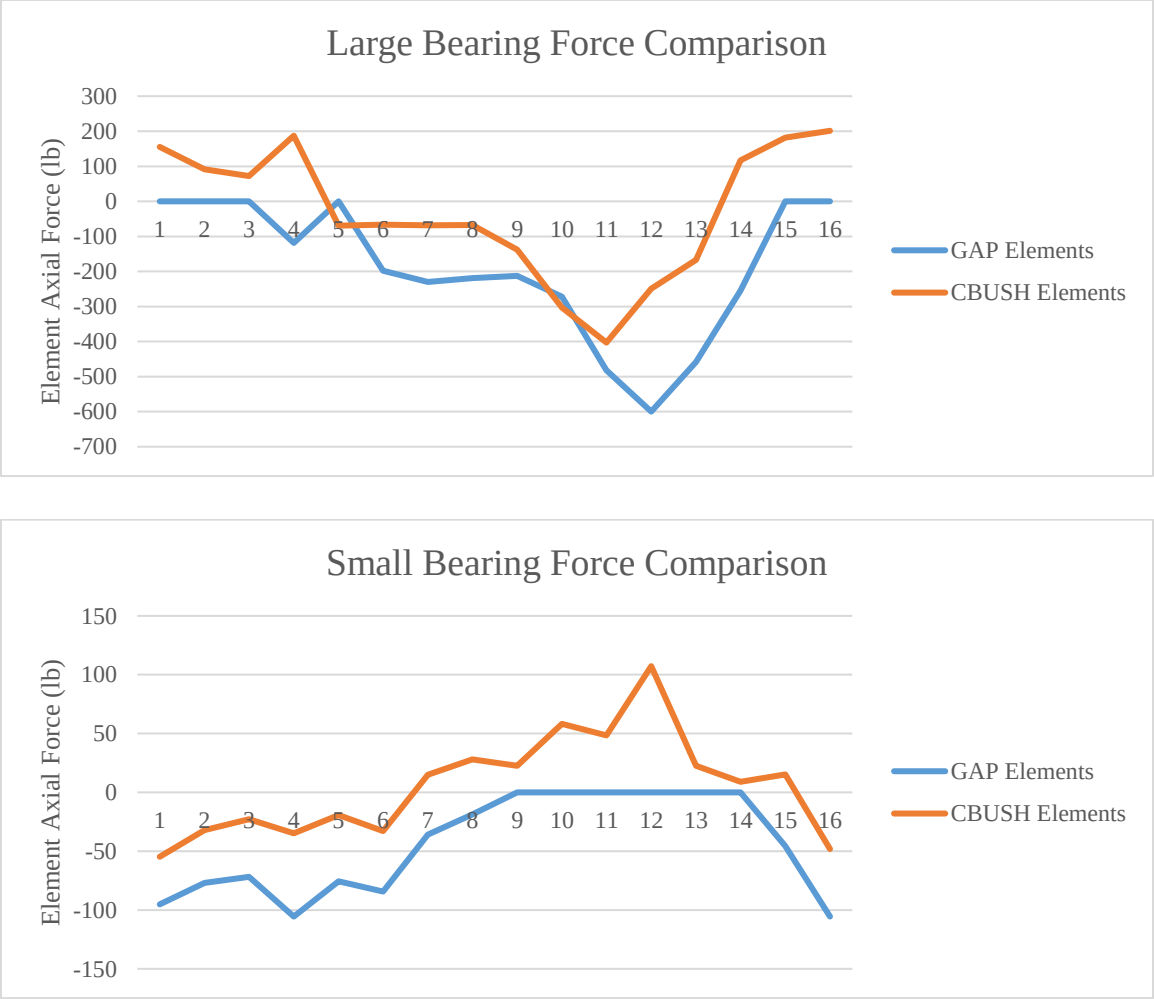

FIGURE 15: DIFFERENTIAL BEARING COMPARISON

	Value	Unit
K1	20	msi
K2	10	msi
K3	1	psi
K4	1	psi
K5	1	psi
K6	1	psi

TABLE 16: CBUSH BEARING PROPERTIES

	Value	Unit
Initial Gap	0	in
Comp. Stiffness	10	msi
Tension Stiffness	0	msi
Transverse Stiffness	10	msi
Y Friction Coeff.	1	
Z Friction Coeff	0	
Preload	0	lbf

TABLE 17: GAP BEARING PROPERTIES

3.4 Inertia Relief Model Validation

The method of inertia relief will be validated here, for the case of a beam bending under its own weight, supported in the middle. This is calculated as an aluminum beam with distributed force. The beam dimensions are 24”x1”x0.125”. The calculations are shown below.

$$\delta_{tip} = \frac{wL^4}{8EI} = .0179"$$

The inertia relief case is setup using CQUAD4 plate elements to create a beam with the same parameters. To represent gravitational loading, a 1g load is applied at the center of the beam. As seen in Figure 16, inertia relief accurately predicts the beam deflection at .0179”.

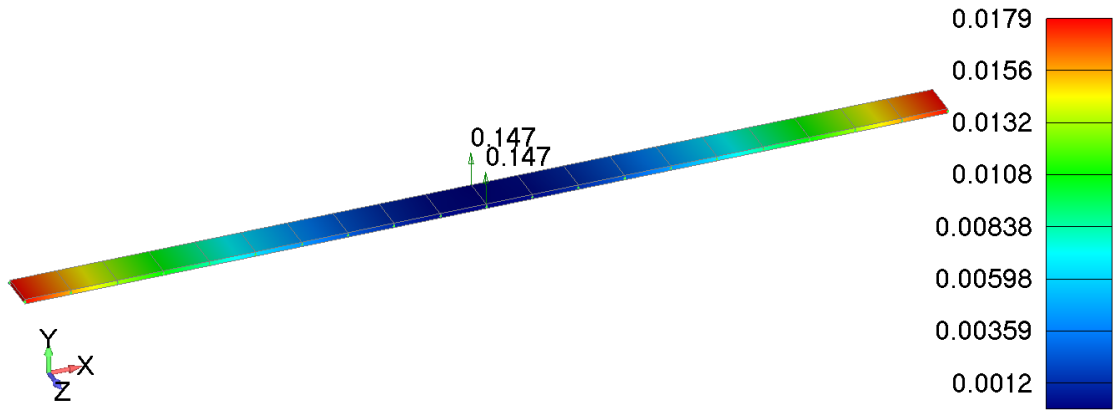

FIGURE 16: INERTIA RELIEF BEAM DEFLECTION

3.5 Discussion

3.5.1 ELEMENT PROPERTIES

The element properties used for mass and metallic structures are straight forward and can be easily verified either with coupon testing or measurement of mass and moment of inertia. The properties used for laminate structures require physical testing to validate their use, hence a combination of test data from internal and external sources is used here. The properties used for CBUSH elements is complex, and strong literature only exists for the shear stiffness values as presented. The combination of properties is validated below.

The properties used for the tire structure are shown to be a reasonable approximation of reality based on the vertical load test performed. However, there is a clear discrepancy of the load distribution, and total load, into the wheel shell between the air and plate only approach. This is likely due to the air model allowing the applied force to be reacted into the wheel shell surface directly, while the plate only approach requires all of the applied load to go through the tire/wheel shell interface.

3.5.2 Modeling Techniques

The modeling techniques presented here generally show good agreement to hand calculations, or more refined analysis techniques. Using CBUSH elements in place of beams, bolt preload, and contact properties proves to capture the bending and translational response within 1.5%. By using 2D laminate elements, the stiffness response of a sandwich panel is captured with 4%. The error for this case could likely be brought down with more accurate material properties to use for analysis, and more physical bending samples tested to get an accurate average. Replacing detailed a 3D mesh with a simplified 2D representations of the suspension clevis results in very good agreement, within 1%. The use of CBUSH element in place of bearings is more difficult to quantify the success of. The correct approach appears to use axial properties as the bearing compressive stiffness and the other properties used to allow proper load transfer through the structure, though in practice this is not straight forward. The results must be scrutinized with sanity checks to ensure the desired outcome is achieved. For instance, for the acceleration load case discussed, the moment applied on the tire is calculated easily based on the applied F_x load and the diameter of the tire. The moment can then be checked at the tripod location and as tension in the chain, to verify that the load progresses through the structure realistically. Additionally, the use of these elements does allow the bearings to pull on the structure, which is unrealistic as bearings only transfer load in compression. A complete application of this technique should include a static, contact driven analysis to determine which elements are in compression. Then, the corresponding CBUSH element should be removed from the analysis.

4 MODEL SETUP

In the following section I will first breakdown the static, aerodynamic, and dynamic portions of the high-level loads into individual tire loads. I will then describe specific model configurations for different driving regimes. Finally, I will give an overview of the model setup and assumptions for each section of the vehicle.

4.1 Loads and Boundary Conditions

In this section I will describe the specific loads and boundary conditions applied to the vehicle analysis. In general, vehicle loads are applied to the wing elements and tire contact patches. Additionally, some internal forces such as brake pedal application are applied. For the vehicle stiffness test, the model is updated to reflect the physical test setup, and loads are applied to the camber plates used. The coordinate system referenced at each contact patch is the vehicle rectangular system. Each area is broken into X, Y, and Z components, to allow application of acceleration, braking, cornering, and normal reaction forces separately. The summary of load cases, and the forces these include, is shown in Table 18 below.

	Acceleration	*Corner Entry*	*Steady State Corner*	*Corner Exit*	*Braking*	*Bump*
Load Case #	2	3	4	5	6	7
Tire 1, 1x lbf		-250			-563	
Tire 2, 1x lbf		-250			-563	
Tire 3, 1x lbf	309			150		
Tire 4, 1x lbf	309			150		
Tire 1, 1y lbf		10	13	8		
Tire 2, 1y lbf		473	591	378		
Tire 3, 1y lbf		12	15	10		
Tire 4, 1y lbf		653	816	522		
Tire 1, 1z lbf	64	99	99	99	225	702
Tire 2, 1z lbf	64	467	467	467	225	702
Tire 3, 1z lbf	216	166	166	166	56	792
Tire 4, 1z lbf	216	534	534	534	56	792
Front Main		155	155	155	155	155
Front Flaps		83	83	83	83	83
Side Main		87	87	87	87	87

Side Flap 1	63	63	63	63	63
Side Flap 2	63	63	63	63	63
Rear Main 1	83	83	83	83	83
Rear Flap 1	44	44	44	44	44
Rear Main 2	83	83	83	83	83
Rear Flap 2	44	44	44	44	44

TABLE 18: LOAD CASES

4.1.1 STATIC FORCES

Static forces come from the weight of the vehicle, and include any effects from load transfer during dynamic events. The vehicle weight comes from the heaviest possible configuration, as this should generate the highest possible loads. This includes the 95th percentile driver as outlined in the rules, and full fluids. This results in a vehicle weight of 343 lbs, and a 220 lb driver. The total weight is then 563 lbs.

The static load is applied with the appropriate weight distribution at each contact patch. This is derived from the static, measured weight distribution of the final car that competed at FSAE-M in 2015. That distribution is 58% rearward weight bias, with 0% left weight bias. As an example, the static load at the front right tire under 1 g load is calculated below. The complete static tire forces can be seen in 0.

$$FR_{static} = Fwt\% \frac{wt_{car} + wt_{driver}}{2} = 0.42 \frac{343 + 220}{2} = 118\ lbs$$

The longitudinal and lateral accelerations are the primary drivers for load transfer effects. Smaller effects include aerodynamic center of pressure migration, wheel travel kinematics, etc. Load transfer is added on top of the static weights, depending on the specific load case. Load transfer is calculated per statics, using the center of gravity of the car and wheel base or track width, depending on the load case being analyzed, as show in the Figure 17 below.

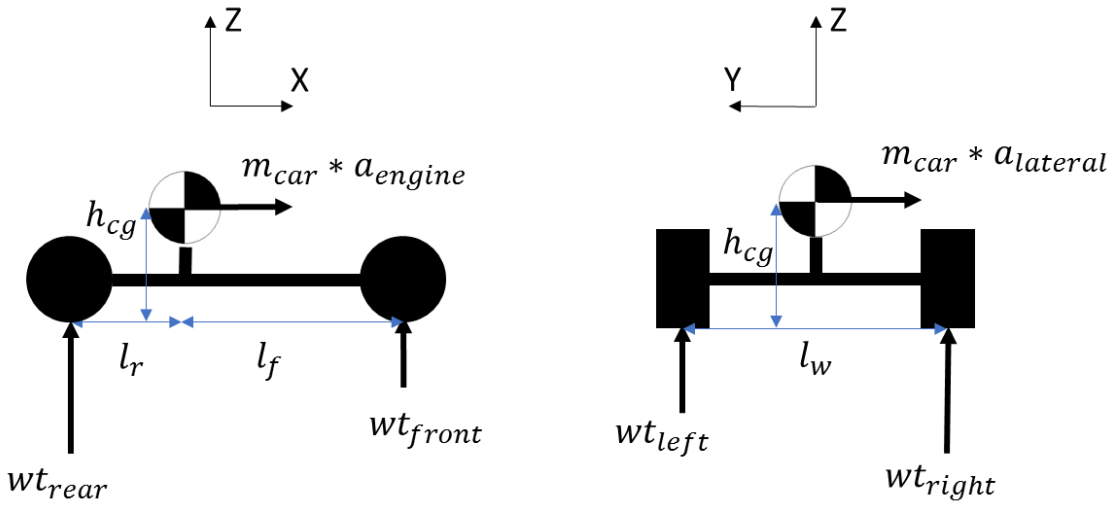

FIGURE 17: LONGITUDINAL AND LATERAL LOAD TRANSFER

An example calculation for the front right tire under 1g engine acceleration is shown below. The load transfer effects, added to the static loads, are shown in detail in 0.

$$FR_{Accel} = FR_{static} - \frac{1}{2} m_{car} a_{engine} \frac{l_r + l_f}{h_{cg}} = 118 - \frac{563}{2} * 1 \frac{11.63}{61.2} = 64.5lbs$$

4.1.2 AERODYNAMIC FORCES

Aero forces are approximated as coarse gradient pressure maps on each wing element, with values chosen to approximate the pressure gradient that exist in CFD simulations. The goal is to capture the total downforce and drag at the worst loading condition. Loads on endplates, and therefore yaw effects, are negated here. 75 mph is used as the maximum speed, as the vehicle is gear limited to that in 5th gear. The pressure input to FEM is shown in Figure 19 below. The pressure values are scaled in the FEM such that x psi equals 1 lb Fz, so the desired downloads can be inputted directly into the model. This is captured in Table 18 in the previous section. These pressures are approximated from the CFD pressure plots, which can be seen in Appendix H.

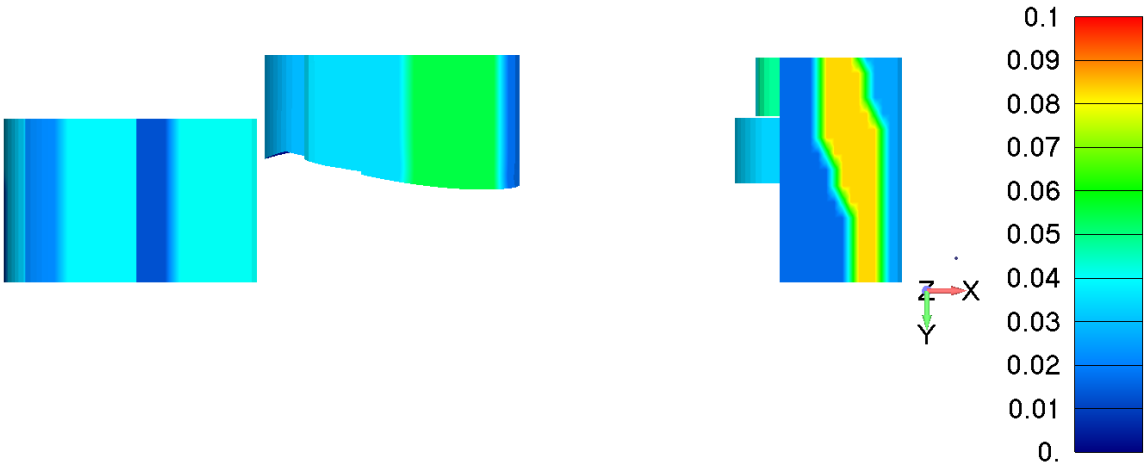

FIGURE 18: AERO PRESSURE CONTOUR, BOTTOM VIEW

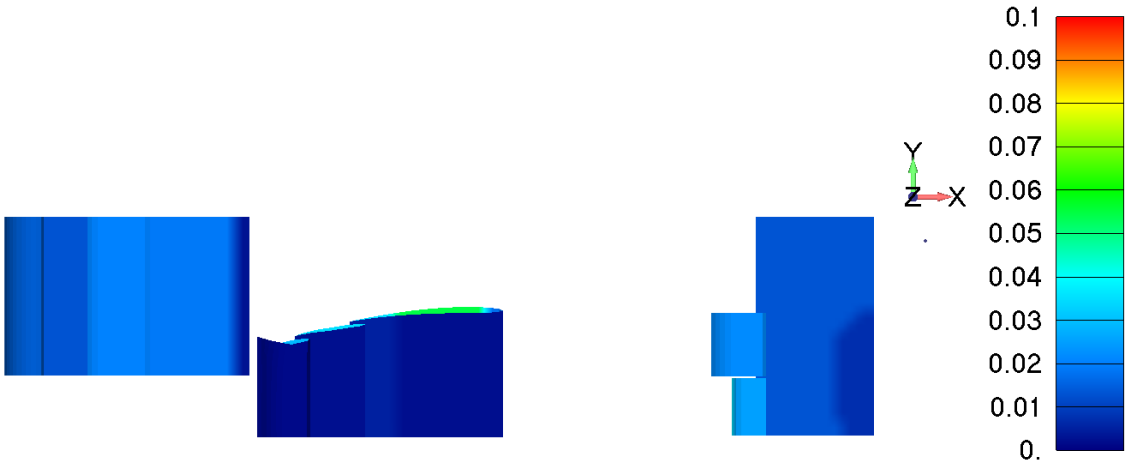

FIGURE 19: AERO PRESSURE CONTOUR, TOP VIEW

The resultant forces are extracted from these pressure distributions. The lift vs drag and center of pressure are calculated below from the Fx, Fz, and My forces extracted from FEM. These are calculated about the vehicle coordinate system. The total forces can be seen below in Table 19.

	Value	Unit
Fx	-156.3	lbs
Fy	0	lbs
Fz	-556.1	lbs
Mx	0.06	lb-in
My	-40610	lb-in
Mz	0.46	lb-in

TABLE 19: TOTAL AERO FORCE

$$\frac{L}{D} = \frac{F_z}{F_x} = \frac{-556.1}{-156.3} = 3.55$$

$$CPx = \frac{My}{Fz} = \frac{-40610}{-556.1} = 73.0$$

$$CP\% = \frac{CPx - CsysOffset}{Wheelbase} = \frac{73 - 39.37}{61.2} = 54.9\%\ Rear$$

To properly apply loads per the free body diagram we also must add in the reaction force at the wheels due to aerodynamic forces to balance the acceleration due to those forces in the Fz direction. The net acceleration in the Fz should be equal to 1g. These are calculated with the CP% shown above, in a similar manner to the static forces previously described. These are shown below in Table 20. These reaction forces are added to any load case where aerodynamic loads are applied.

		Value	Unit
DF @ mph	v	75	mph
Tire Fz loads	FL	130.8	lb
	FR	130.8	lb
	RL	147.5	lb
	RR	147.5	lb

TABLE 20: AERO REACTION FORCES

4.1.3 DYNAMIC FORCES

The cornering, bump, acceleration and deceleration forces are covered in this section, based on overall vehicle performance goals discussed previously. They are summarized earlier in Table 6. Acceleration and deceleration forces are assumed to be evenly

distributed left to right across the vehicle. This is acceptable due to the center of gravity of the car being nearly centered in the ZX plane. Lateral forces are assumed to be only on the outside tires, to create the highest load scenario where all the cornering force is on two tires. These forces are distributed to individual tires based on an assumption of steady state cornering, and vehicle center of gravity location. Bump forces are assumed to be only on 1 tire, to create the worst-case loading condition. This is applied to Tire 2 and 4, with 1 and 3 covered due to symmetry. The tire forces due to dynamic effects are summarized below in Table 21.

Dynamic Loads	Tire	Load	Component
Steady State Cornering	1	0	-
	2	591	Fy
	3	0	-
	4	816	Fy
Acceleration	1	0	-
	2	0	-
	3	309	Fx
	4	309	Fx
Braking	1	563	Fx
	2	563	Fx
	3	0	-
	4	0	-
Engine Braking	1	0	-
	2	0	-
	3	253	Fx
	4	253	Fx

TABLE 21: DYNAMIC TIRE FORCES

4.1.4 STIFFNESS TEST FORCES

The hub to hub forces applied for the torsional stiffness load case follow exactly from physical testing. Any load however will work, as the model is linear elastic. The maximum load is selected to allow verification with the highest loaded condition. These loads and calculated moments are shown below.

	Value	Unit
Track	46.1	in
Front Force	229	lb
Rear Force	317	lb
Front Moment	10556	lb-in
Rear Moment	14613	lb-in

TABLE 22: TORSION TEST FORCES

The toe and camber stiffness load case forces and calculated moments are shown in the table below. The camber force is applied to the camber plate, while the toe force is applied through an RBE2 into the camber plate to simulate turning the plate 90 degrees.

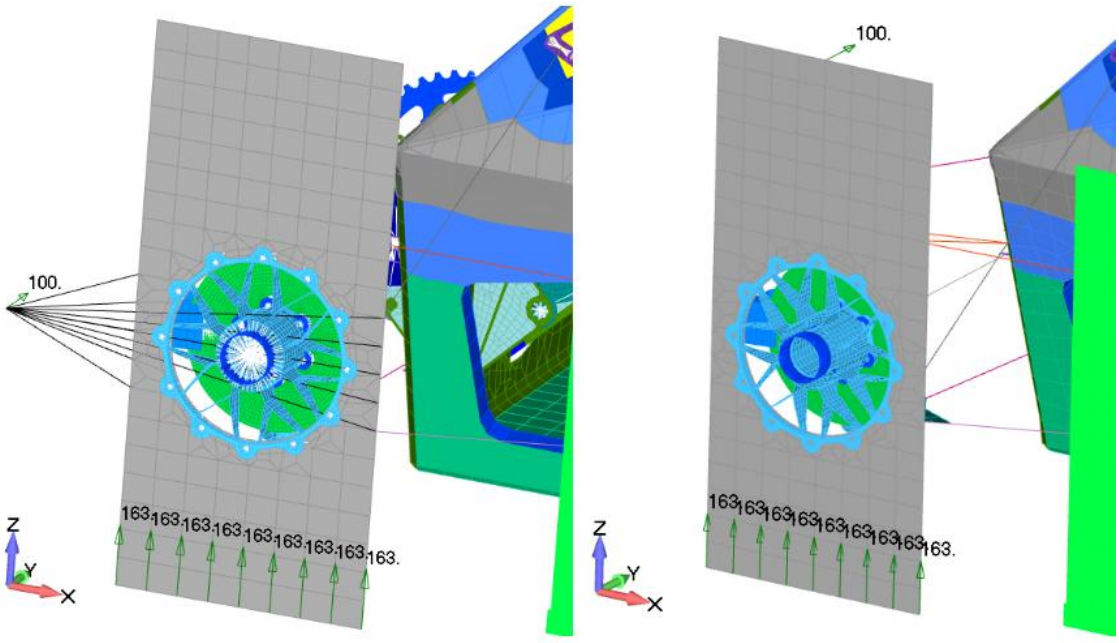

FIGURE 20: SUSPENSION TEST FEM

	Value	Unit
Arm	9	in
Force	100	lb
Moment	900	lb-in

TABLE 23: SUSPENSION TEST FORCES

4.1.5 Boundary Conditions

In this section I will discuss the overall mass of the vehicle represented in FEM, and the specific analysis configurations used. The specific approximations of mass are covered in the Mass section. The total mass and center of gravity coordinates are shown below in Table 24. The inertia of the vehicle is shown below in Table 25. This is directly output from FEM, based on the modeled geometry.

	Mass (lbm)	Center of Gravity in Vehicle Coordinates (in)		
		X	Y	Z
Structural	507.1	-73.1	-0.01	11.0
Nonstructural	56.2	-68.3	0	16.7
Total	563.3	-72.6	-0.01	11.5

Table 24: Vehicle CoG Location

Inertias in Vehicle Coordinates	Ixx	Iyy	Izz	Ixy	Iyz	Izx	Units
About Vehicle Origin	2.16E+05	3.33E+06	3.30E+06	7.87E+02	-2.54E+02	-4.96E+05	lb-in^2
About CG Location	1.40E+05	2.83E+05	3.31E+05	1.29E+02	-1.49E+02	-2.14E+04	lb-in^2

Table 25: Vehicle Mass MOI

Further, boundary conditions exist within the model itself. For different load regimes, different element configurations are used to represent reality. The first group is used for acceleration, cornering, and bump load cases. This group fixes the rotation of Tires 1 and 2 to stabilize the analysis. This is acceptable because the loads applied in Fx for these load cases is effectively zero. The second group is used for braking load cases. This group releases the rotation of all tires about their spindles, but adds a connection from the brake caliper to brake rotor. This allows the load to go through the upright in a realistic way. The third group is used to represent the physical stiffness test setup. This group replaces the tires and wheel shells with wheel setup plates. Two of these groups can be seen in Figure 21 below.

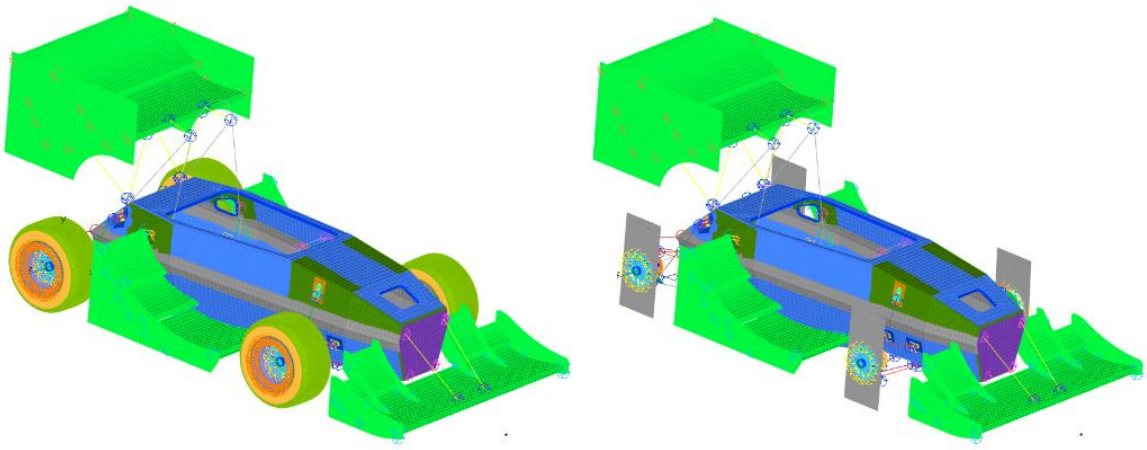

FIGURE 21: CORNERING AND TORSION TEST CONFIGURATION

4.2 Sub System Modeling

4.2.1 CHASSIS AND AERO

In this section, the finite element modeling of the chassis and aero system are discussed. In general, all composite parts are imported into FEMAP as an IGES surface, and meshed using the automatic mesher within FEMAP, with a specified element size of 1 inch. Roll hoop and wing support struts are modeled as beam elements with the appropriate sizes. All bolted connections are made using CBUSH elements, with properties calculated using the equations previously discussed. The joint between the upper and lower half of the carbon monocoque is a double lap butt joint. Because of its comparatively low stiffness, the adhesive used in this joint is not represented in FEM. Instead, all forces transferred through the joint is carried through the carbon fiber strap. There are many other assumptions made to simplify the model. The roll hoops are simplified to a single element at each connection point with the chassis, the plate tabs on the roll hoop are not included in the analysis model. Small hardpoints in the wing elements are not included in the laminate representation. The strap glue properties are shown in Table 26 below.

	Value	Detail
Glue Type	1	Spring
Eval Order	2	Medium
Refine Source	2	Refinement Occurs
Penalty Factor	2	Force per Length X Area
Normal Factor	615000	
Tangential Factor	212000	

TABLE 26: GLUE CONNECTION PROPERTIES

4.2.2 INBOARD SUSPENSION AND STEERING

In this section, the suspension links, inboard clevises, roll bars, and steering system modeling is discussed. There are a few critical simplifications made to the inboard suspension to limit the number of elements used to run the analysis and simplify the model construction. All tube based structures are represented by beam elements with appropriate properties. All clevises are modeled using 2D plate elements. Most bolted connections are modeled using CBUSHs with stiffness values calculated as previously discussed, however, at spherical bearing connections the bolt is replaced with an RBE2 element. The vehicle springs are represented using CBUSHs, with the axial stiffness directly representing the spring stiffness. The steering pinon gear is not modeled directly, but the connection is approximated with a CBUSH element. The specialized properties for these connections are shown in Table 27 below.

Inboard Suspension Properties

	Spherical	Front Springs	Pinion Gear
K1	1.50E+07	7.00E+02	5.00E+06
K2	1.50E+07	1.00E+05	5.00E+07
K3	1.50E+07	1.00E+05	5.00E+07
K4	1.00E+00	1.00E+05	1.00E+04
K5	1.00E+00	1.00E+05	1.00E+02
K6	1.00E+00	1.00E+05	1.00E+02

TABLE 27: INBOARD SUSPENSION PROPERTIES

4.2.3 Outboard Suspension

In this section, the modeling of the upright, spindle, brakes, and wheel center is discussed. The Outboard suspension is greatly simplified as it is a complex assembly. These components are made with isotropic materials, and are represented with 2D plate elements. The simplifications and model implementation are both made to accurately reflect the system stiffness. The connections between components are made with CBUSH elements, with varying properties to properly constrain and release motion to reflect reality. These are shown in Table 28 below.

Outboard Suspension Properties

	Spindle Bearings, Front	Spindle Bearings, Front, Released	Spindle Bearings, Rear, Released	Brake, Released	Brake, Locked
K1	2.00E+07	2.00E+07	2.00E+07	1.00E+07	1.00E+07
K2	1.00E+07	1.00E+07	1.00E+07	1.00E+00	1.00E+08
K3	6.00E+05	1.00E-01	1.00E-01	1.00E+00	1.00E+08
K4	6.00E+05	6.00E+05	6.00E+04	1.00E+02	1.00E+02
K5	6.00E+05	1.00E-01	1.00E-01	1.00E+00	1.00E+06
K6	6.00E+05	6.00E+05	6.00E+04	1.00E+00	1.00E+06

TABLE 28: OUTBOARD SUSPENSION PROPERTIES

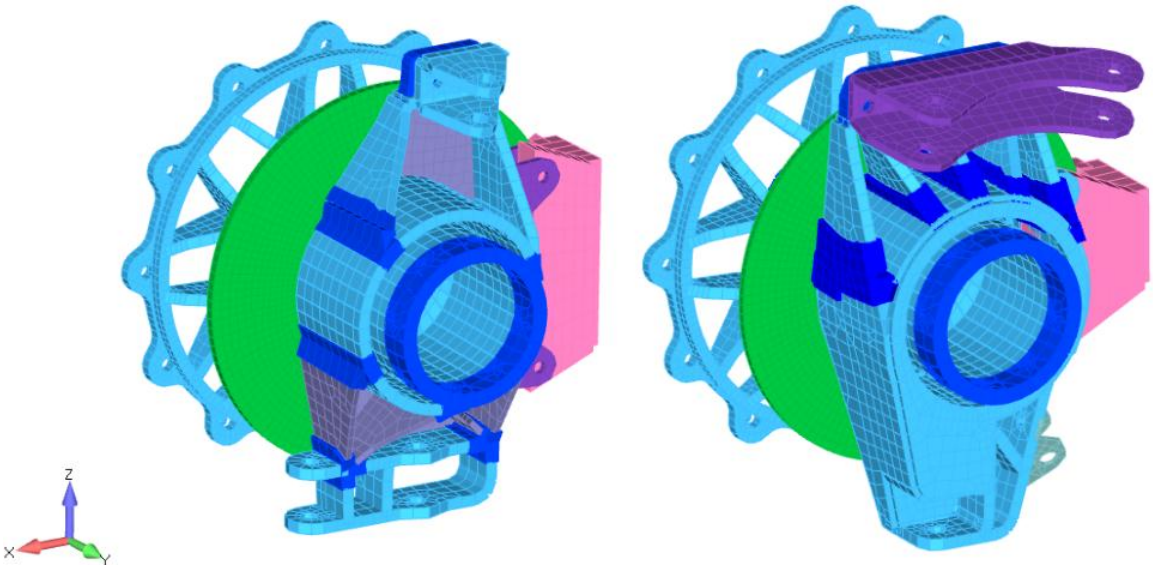

FIGURE 22: FRONT AND REAR SUSPENSION OUTBOARD

The general model structure is as follows, from inboard connection to contact patch. The outboard clevis is like the inboard clevis, with a spherical CBUSH and RBE2 element tying the wings of the 2D plate elements together. The outboard clevis is connected to the upright with a CBUSH and RBE2 elements with stiffness properties as previously discussed. The upright is modeled using 2D plate elements. The upright is connected to the spindle with CBUSH elements representing the spindle bearings, which use the Young's modulus of steel for their axial stiffness; other properties are determined based on how motion is constrained in the system. The spindle is constrained axially with CBUSH elements that represent the outer wheel nut, and inner spindle nut. The wheel center is then connected to the same wheel nut element axially, and CBUSH elements representing wheel pins radially. The brake rotor is connected directly to the spindle with RBE3 elements. For Braking load cases, a connection between the brake caliper and brake rotor is included.

4.2.4 TIRES

In this section, modeling of the wheel shell and tire are discussed. This starts at the wheel center to wheel shell connection, with is done with CBUSH and RBE2 elements with calculated joint stiffness. The wheel shell is meshed using 2D plate elements. The wheel shell to tire connection is made using a string of similar stiffness CBUSH elements. As these elements are generated automatically within FEMAP and their specific orientation is unknown, the same stiffness is used for each degree of freedom. The tires are then modeled using 2D plate elements, with properties as previously discussed.

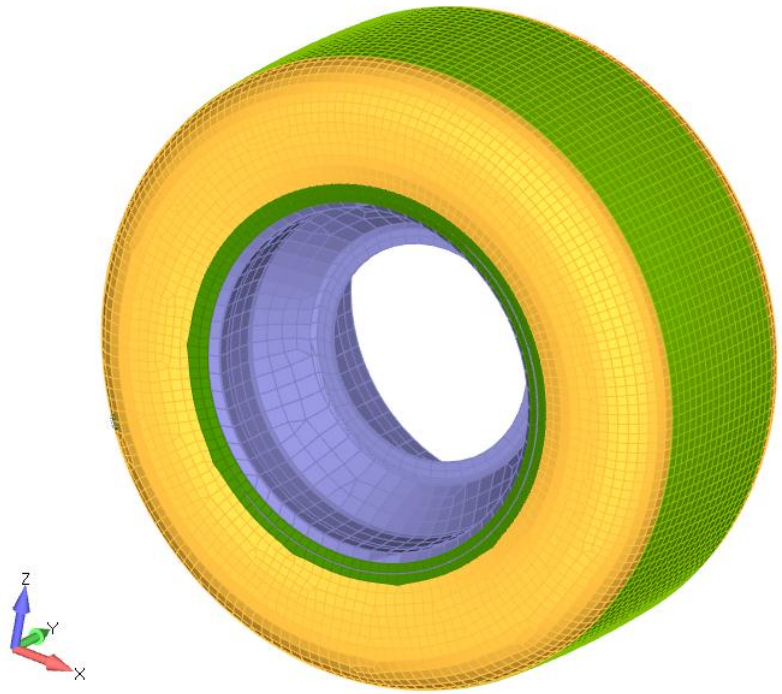

FIGURE 23: TIRE AND WHEEL SHELL

4.2.5 DRIVETRAIN

In this section, the drivetrain system modeling is discussed. The engine is central to this system, and is included in this analysis as an RBE2 element. The mass of the engine is represented with a single mass element as previously discussed. The engine is connected to the engine mounts with CBUSH elements. The front and rear engine mounts are represented by 2D plate elements. They are connected to the chassis with RBE2/3 and CBUSH elements. The upper engine mount is represented with beam elements. The rear engine mount is also connected to the differential mount, which is modeled with 2D plate elements. The differential is connected to the mounts in an equivalent way as the spindle to upright connection, with CBUSH elements. The tripods are modeled with CBUSH elements, and connect directly to the driveshaft beam elements.

Differential Properties			
	Diff Bearings	Tripod, Axial Fixed	Tripod
K1	2.00E+07	1.00E+06	5.00E+01
K2	1.00E+07	2.00E+07	2.00E+07
K3	1.00E-01	2.00E+07	2.00E+07
K4	1.00E+04	2.00E+07	2.00E+07
K5	1.00E-01	1.00E+00	1.00E+00
K6	1.00E+04	1.00E+00	1.00E+00

TABLE 29: DIFFERENTIAL PROPERTIES

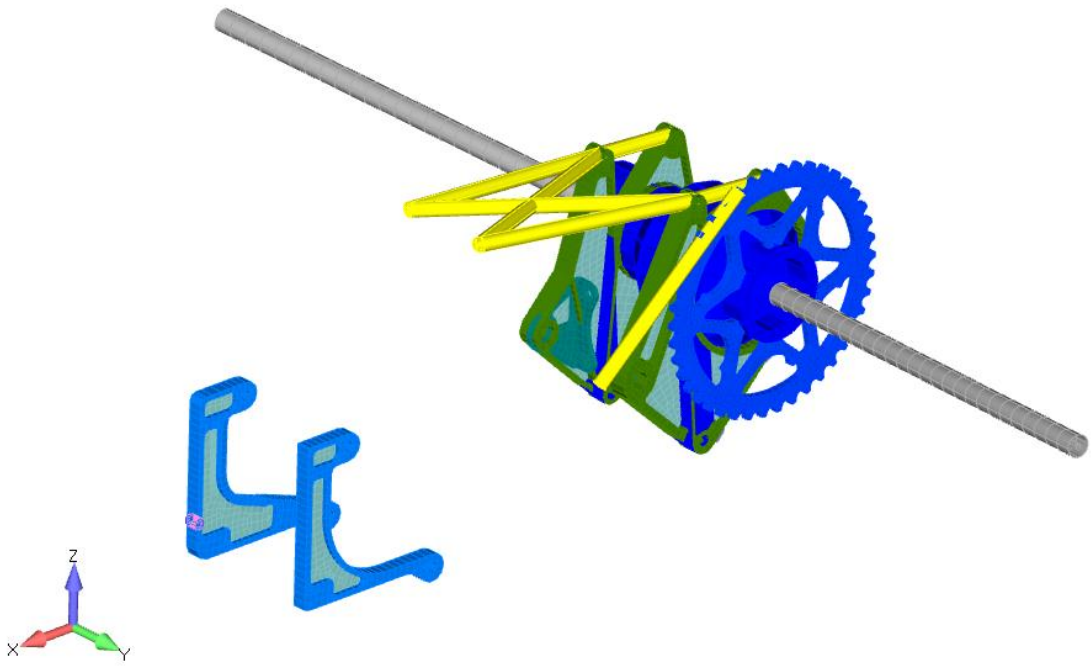

FIGURE 24: DRIVETRAIN

4.2.6 MASS

For analysis constrained with inertial relief, it is imperative that the mass of elements is accurate. While it is trivial to input the appropriate densities for metallic components or measured ply weights for composites, what is not trivial is to end up with an accurate total mass and CG location. For every simplification made in the model, it is necessary to add mass in that location to represent the mass lost. It is also necessary to properly tie this

mass into the structure so that the effects of it are properly accounted for. The properties for mass elements have already been discussed, and they are tied into the analysis model with RBE3 elements at an appropriate location. All mass elements used are shown in Figure 25 below.

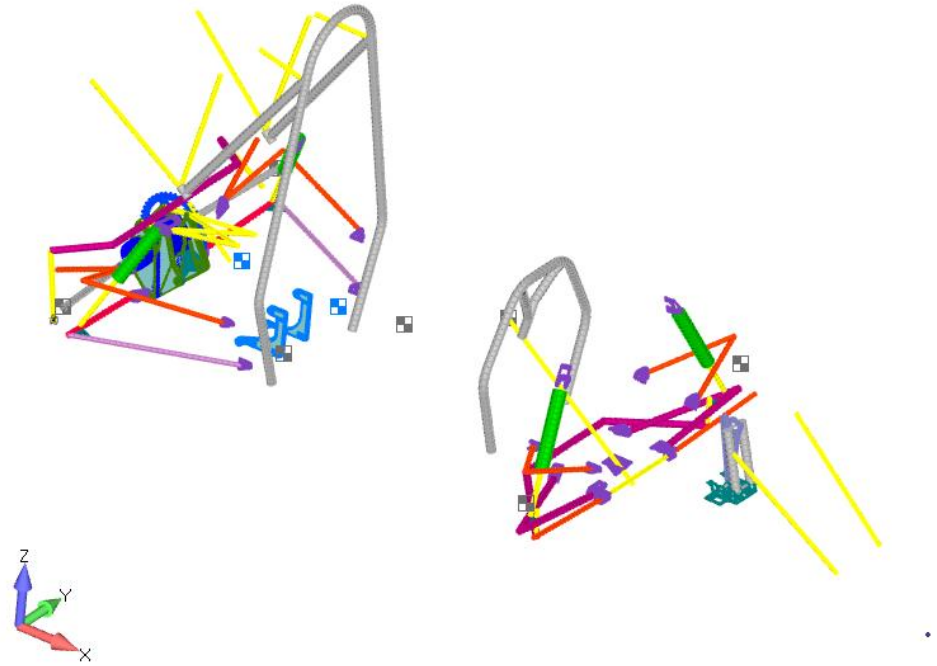

FIGURE 25: MASS ELEMENT LOCATIONS

4.3 Discussion

4.3.1 LOADS

The load inputs to FEM presented here come directly from the overall performance of the vehicle. This is validated from on track data. The methods used are rudimentary in nature, and could be further refined. For instance, the front and rear load distribution during corner could be evaluated including the torsional stiffness of the frame. Additionally, the loads are applied relative to the vehicle coordinate system. This results in small errors, as the actual force is relative to the tire coordinate system and this changes relative to the chassis depending on suspension travel. The outboard suspension

could be translated relative to the frame for different load levels to compensate for this. Finally, the aerodynamic loads do not include any forces on the endplates. While this is reasonable for straight line cases such as maximum breaking, these effects should be added to cornering load cases.

4.3.2 MODEL

The chassis and aerodynamic element models come directly from the mold line surfaces of the parts they represent. While this is easy to implement, there are shortcomings. The in-plane forces that result is not totally correct, as the laminate midplane is not in the actual location. Additionally, it is reasonable to exclude the adhesive layer between the chassis halves, because this layer much less stiff than the surrounding carbon fiber straps. The suspension and steering system modeling comes from midplane surfaces of the corresponding parts, as well as tube geometry. As the properties come directly from isotropic materials, it is assumed that these are very good representations. The steering system includes a unique CBUSH element to represent the pinion gear. This results in locked steering, and provides an element that can be used to extract the moment the driver feels on the wheel during cornering. The outboard suspension and differential includes CBUSH elements that represent the large bearings in these systems. It appears that their function is reasonable, although their comparison to contact models is not great. This could be an area for refinement. Additionally, the tire models are very approximate. Further physical testing, especially in measuring their lateral stiffness, could be used to develop a more refined structural model.

5 RESULTS AND DISCUSSION

5.1 Overall Dynamic Results

The following are the enveloped results from all dynamic load cases. A subset of suspension, aero, and powertrain forces is presented, along with their driving load case. Link forces are presented as just the axial component; bending forces, if present, are not shown here. Expect where indicated, the results shown are for bolted connections and are

presented as axial force and shear force (calculated as the root sum of squares of the in-plane forces). All forces are presented in units of lbf, and moments are in units of in-lb. Following, in Figure 26 through Figure 29, the stress in a few key components is shown. The chassis principal stress and core shear stress is shown, along with a plot illustrating what load cases drive different areas of the frame.

Front Suspension		
	Link Force	Load Case
Shock spherical	841.7	Bump
FUF	759.3	Braking
FUR	759.7	Braking
FLF	2647.9	Braking
FLR	2964.2	Braking
Front Tie Rod	345.3	Braking

TABLE 30: FRONT SUSPENSION RESULTS

Rear Suspension		
	Link Force	Load Case
Shock spherical	383.0	Bump
RUF	198.0	Accel
RUR	479.7	SS Corner
RLF	197.1	Bump
RLR	905.3	SS Corner
Toe Link	359.0	Accel

TABLE 31: REAR SUSPENSION RESULTS

Suspension Clevis Bolts				
	Tension	Load Case	Shear	Load Case
Front Shock	647.0	Bump	484.9	Bump
Front Upper	622.8	Braking	374.2	Braking
Front Lower	3375.6	Braking	2564.7	Braking
Rear Shock	519.9	Bump	300.6	Bump
Rear Front	244.3	Bump	150.7	Accel
Rear Back	920.9	SS Corner	483.2	SS Corner

TABLE 32: SUSPENSION CLEVIS RESULTS

Powertrain				
	Axial	Load Case	Shear	Load Case
Chain Tension	1307.2	Accel	N/A	N/A
Engine, Upper Mount	549.7	Accel	N/A	N/A
Engine, Front Upper	37.9	SS Corner	175.3	Accel
Engine, Front Lower	200.5	SS Corner	285.6	SS Corner
Engine, Rear	3787.9	Accel	786.0	Accel
Left EM	290.8	Accel	146.3	SS Corner

Right EM	235.5	Accel	137.3	SS Corner
Diff Mount, Left	172.7	SS Corner	216.6	Accel
Diff Mount, Right	178.9	SS Corner	139.0	SS Corner
	Moment	Load Case		
Tripod	2590.5	Accel		

TABLE 33: POWERTRAIN RESULTS

Aero Mounts

	Axial	Load Case	Shear	Load Case
Front Wing, IA	116.6	Bump	135.7	Corner Exit
Side Wing Main	92.8	SS Corner	68.4	Bump
	93.4	Bump	16.8	SS Corner
	67.0	SS Corner	17.7	SS Corner
Side Wing Mid	113.8	SS Corner	20.7	Bump
	97.8	SS Corner	18.2	Bump
	77.5	Bump	17.0	Bump
Side Wing Upper	0.0	Bump	0.0	Accel
	148.1	Corner Entry	26.8	Corner Entry
	169.7	Corner Entry	37.3	SS Corner
	Link Force			
Front Wing Strut	75.8	Bump		
Rear Wing Upper Strut	271.6	Corner Entry		
Rear Wing Mid Strut	105.5	Corner Exit		
Rear Wing Lower Strut	162.8	Corner Entry		

TABLE 34: AERO MOUNT RESULTS

Driver Interface

	Axial	Load Case	Shear	Load Case
Pedal Base	1472.5	Braking	615.3	Braking
Pedal Compression	457.1	Braking	3.0	Braking
Pedal Base	204.4	Braking	2.5	Braking
	Moment			
Steering Wheel	31.7	Braking		

TABLE 35: DRIVER INTERFACE RESULTS

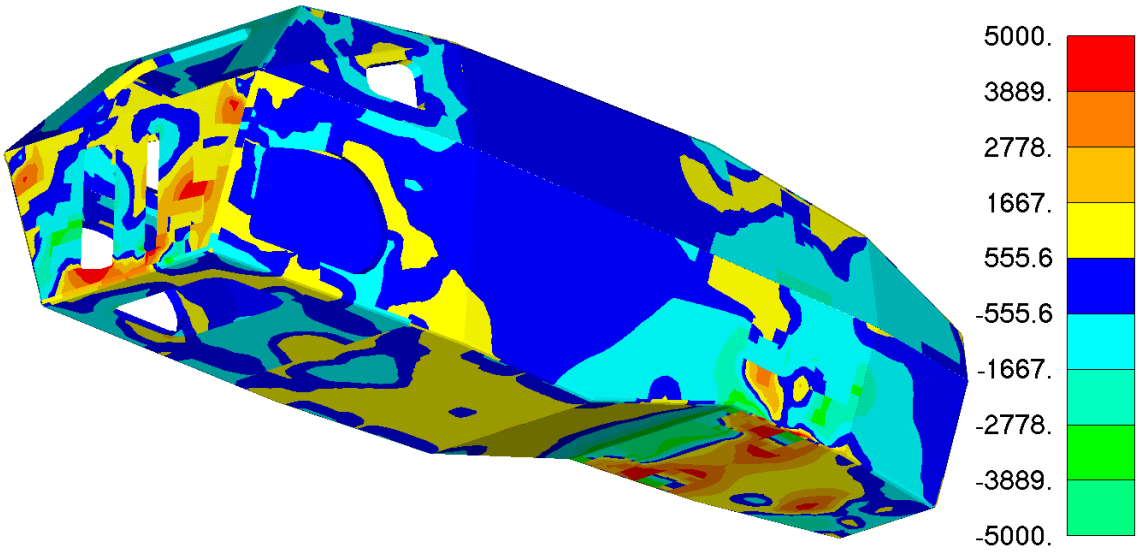

FIGURE 26: PRINCIPAL STRESS ENVELOPE

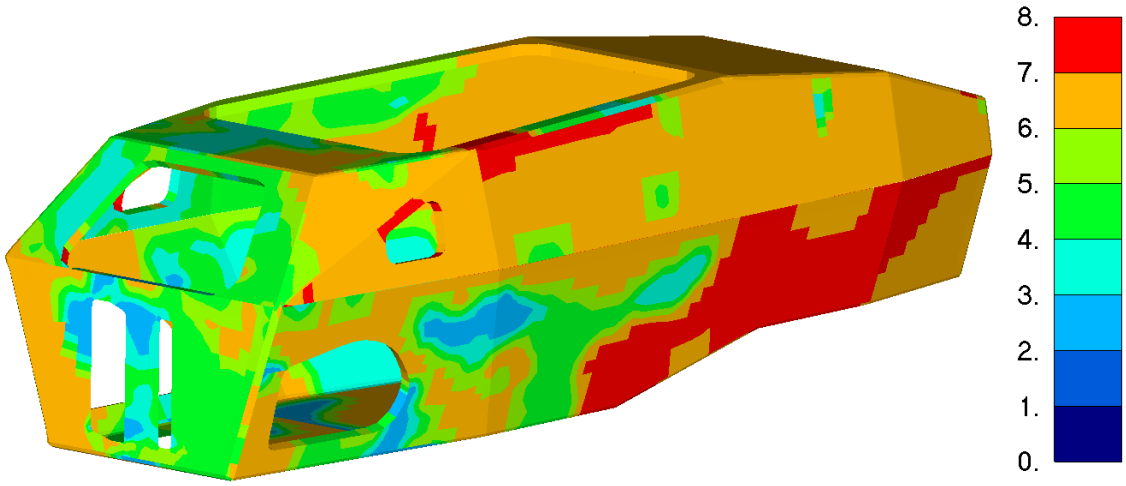

FIGURE 27: PRINCIPAL STRESS DRIVING LOAD CASES

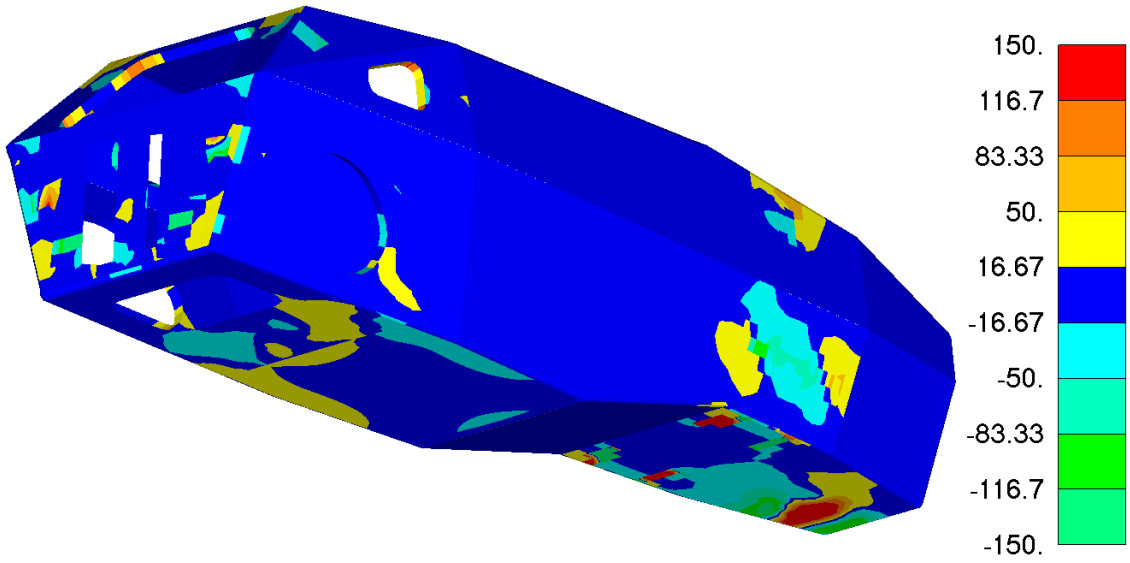

FIGURE 28: SHEAR STRESS ENVELOPE

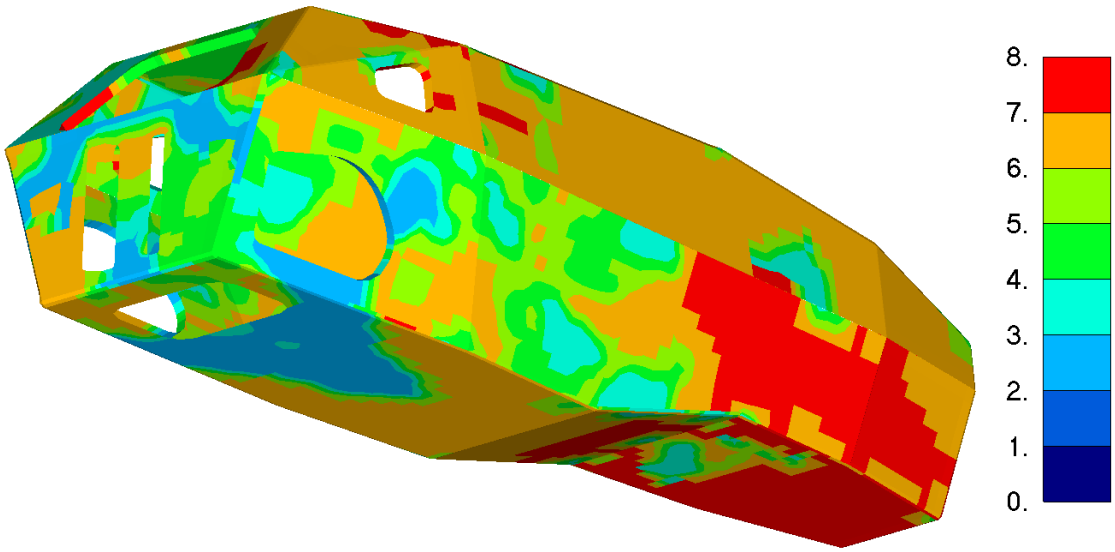

FIGURE 29: SHEAR STRESS DRIVING LOAD CASES

5.2 Detailed Results and Discussion

In this section, the forces used for analysis are discussed. Then, the individual load cases and their results are presented and discussed. Specific areas of interest are shown including laminate and metallic displacement and stress results, depending on the driving area of each load case.

5.2.1 Dynamic Results

5.2.1.1 Acceleration Results and Discussion

These loads are intended to represent a standing start, full force acceleration. The focus area of the chassis is the engine mounts and rear suspension. The component focus is the drivetrain, sprocket, and engine mounts. The primary model check for this load case is the chain tension force, which is 1307 lbf. It makes sense that the most suspension links are not driven by this load case, as the driving moment is applied through bearings that offer no resistance to this torque.

	Force (lbf)
Shock	60
FUF	2
FUR	22
FLF	54
FLR	27
Tie Rod	16

Table 36: FR Accel Results

	Force (lbf)
Shock	112
RUF	198
RUR	123
RLF	156
RLR	297
Toe Link	359

Table 37: RR Accel Results

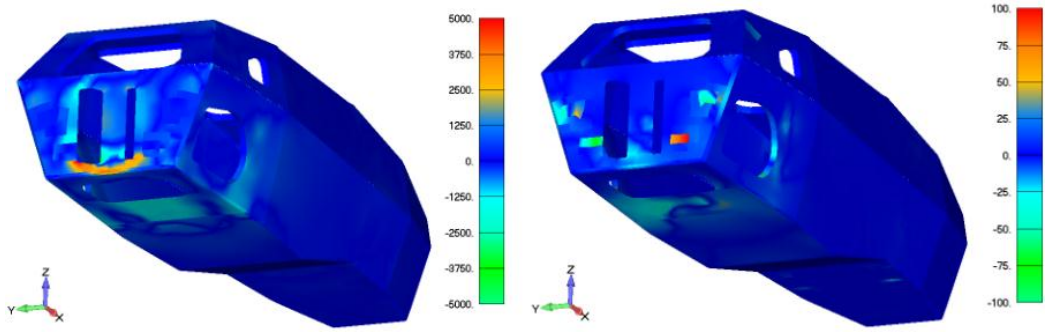

Figure 30: Accel Principal and Shear Stress

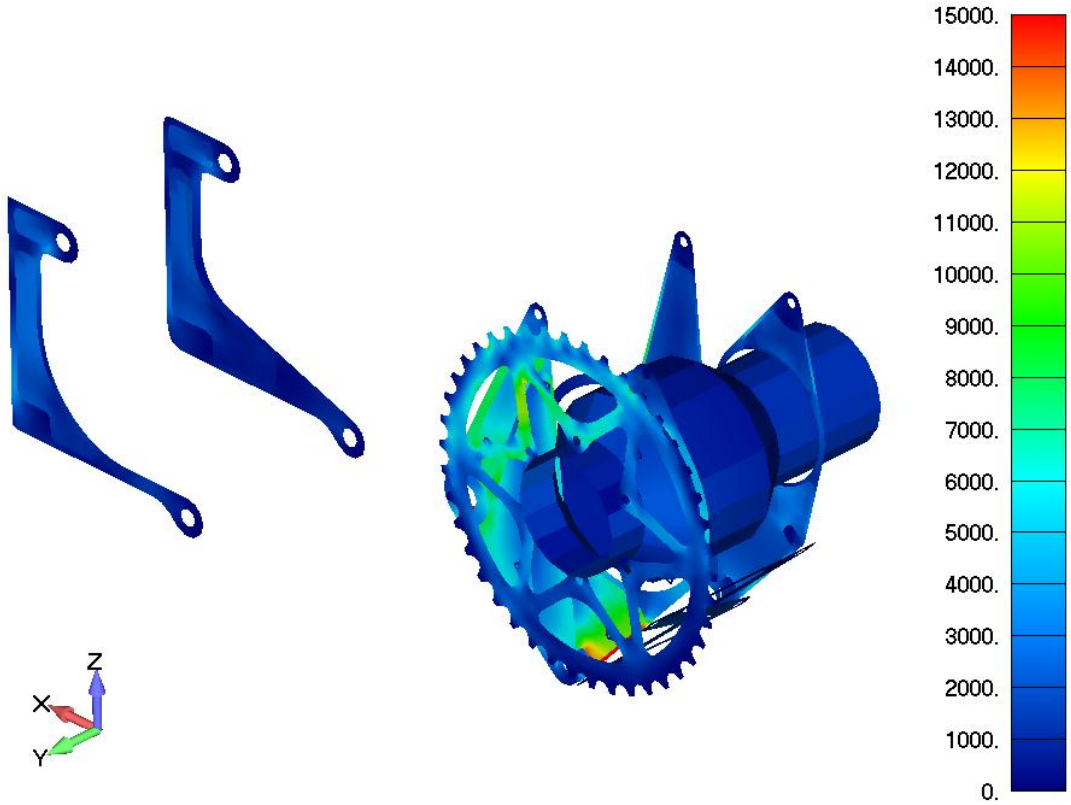

FIGURE 31: DRIVETRAIN VON MISES STRESS

5.2.1.2 Corner Entry Results and Discussion

This load case represents the braking and turning that can occur during the transition into a corner. It is reasonable that no suspension link forces are driven by this load case, as the applied loads are only scaled versions of the braking and steady state case. It is interesting that this load case drives a small region of the chassis between the front upper suspension mounts.

	Force (lbf)
Shock	540
FUF	359
FUR	437
FLF	1162
FLR	1239
Tie Rod	244

TABLE 38: FR CORNER ENTRY RESULTS

	Force (lbf)
Shock	187
RUF	33
RUR	354
RLF	40
RLR	633
Toe Link	69

TABLE 39: RR CORNER ENTRY RESULTS

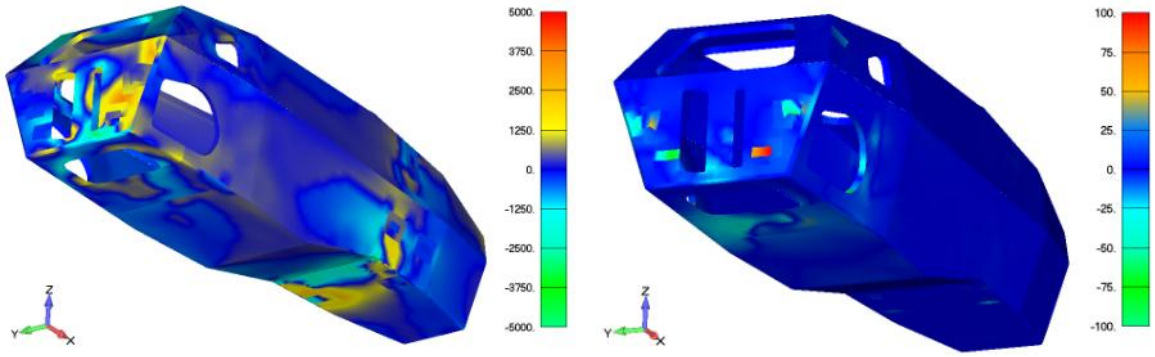

FIGURE 32: CORNER ENTRY PRINCIPAL AND SHEAR STRESS

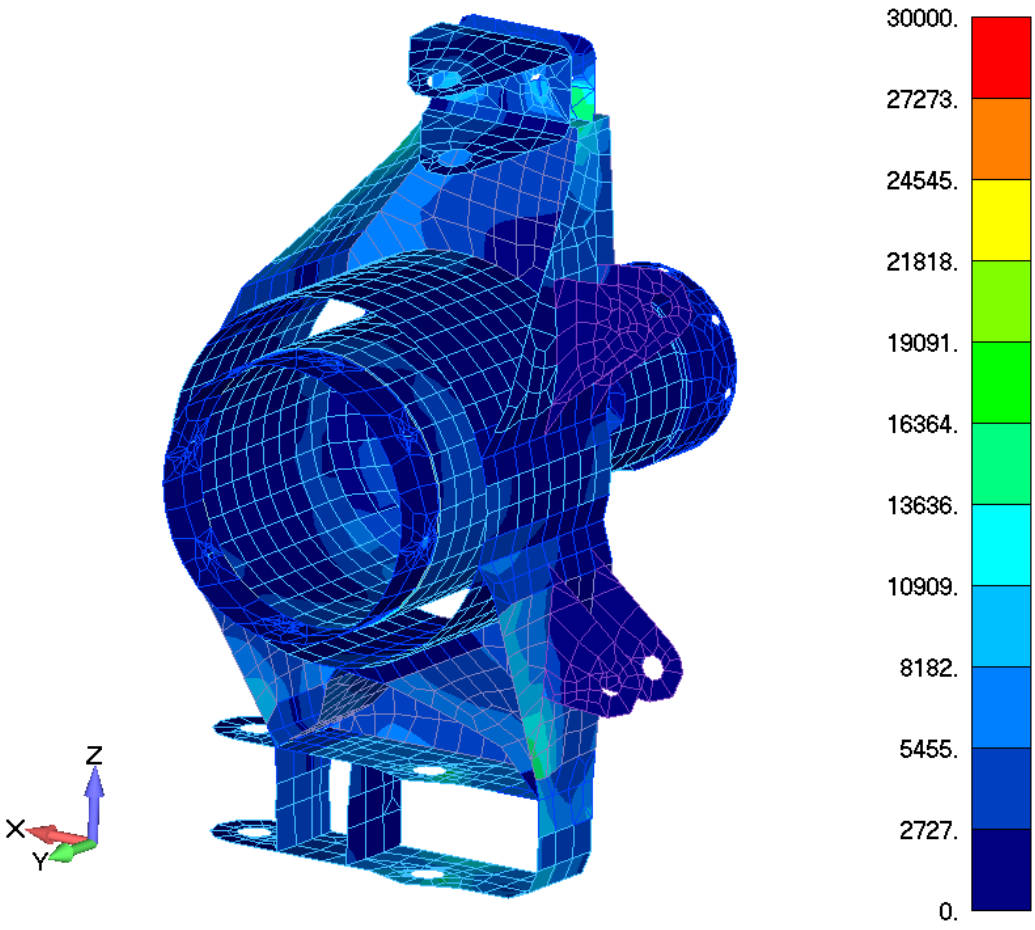

FIGURE 33: CORNER ENTRY VON MISES STRESS

5.2.1.3 Steady State Corner Results and Discussion

This load case represents the steady state lateral acceleration that occurs during a corner. It is interesting that this case only drives one main region, the rear suspension mounts. This is reasonable when one considers that this load case provides the maximum lateral force on the vehicle, and the two rear suspension links are close to parallel with the load application.

	Force (lbf)
Shock	524
FUF	259
FUR	133
FLF	971
FLR	228
Tie Rod	118

TABLE 40: FR S.S. CORNER RESULTS

	Force (lbf)
Shock	188
RUF	63
RUR	480
RLF	61
RLR	905
Toe Link	45

TABLE 41: RR S.S. CORNER RESULTS

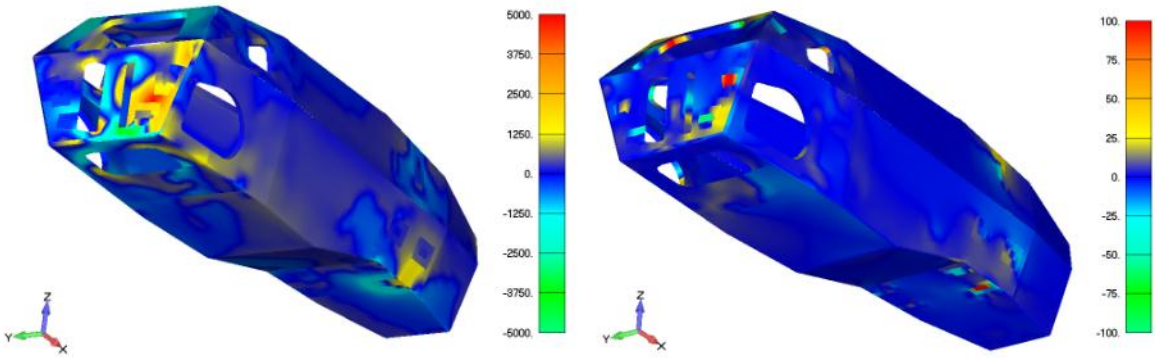

FIGURE 34: S.S. CORNER PRINCIPAL AND SHEAR STRESS

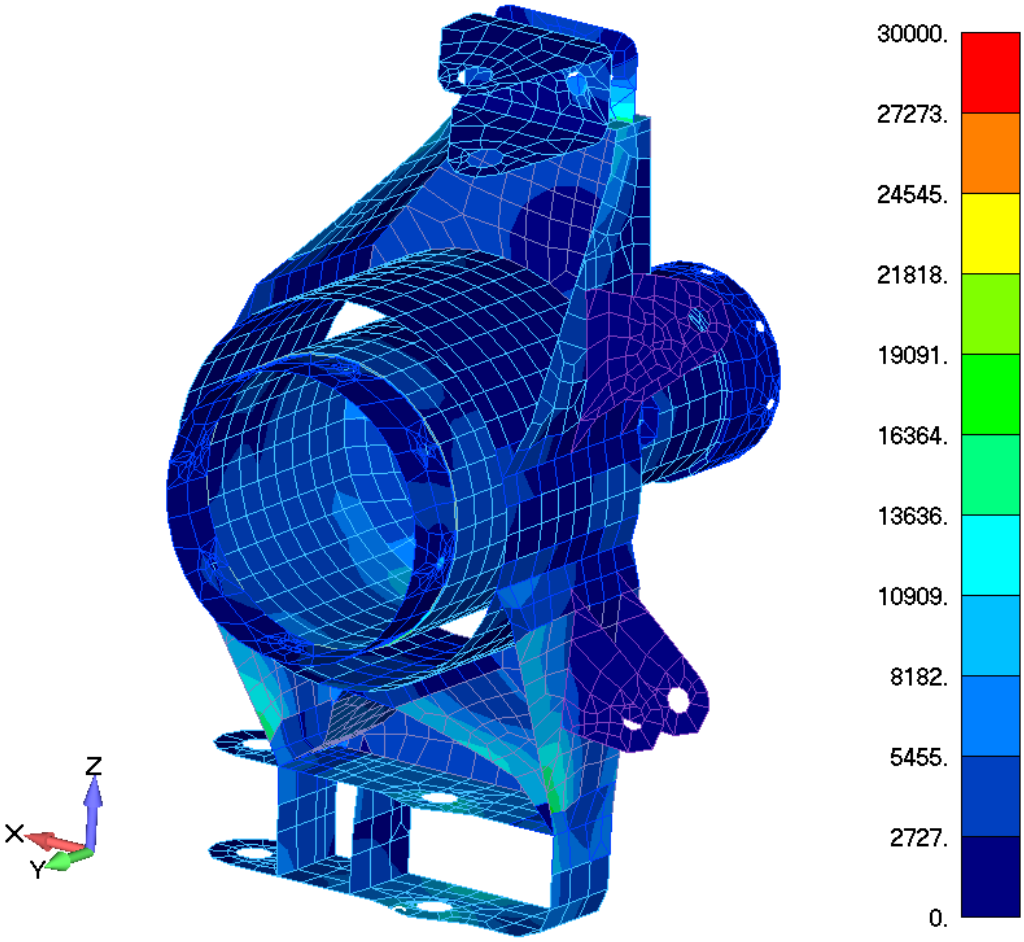

FIGURE 35: S.S. CORNER VON MISES STRESS

5.2.1.4 Corner Exit Results and Discussion

This load case represents the lateral force and acceleration that occurs at the exit of a corner. While this case does not drive any specific connections, it is interesting that it does contribute the most laminate stress to the region near the driver.

	Force (lbf)
Shock	502
FUF	132
FUR	71
FLF	529
FLR	186
Tie Rod	68

TABLE 42: FR CORNER EXIT RESULTS

	Force (lbf)
Shock	209
RUF	104
RUR	279
RLF	36
RLR	356
Toe Link	219

TABLE 43: RR CORNER EXIT RESULTS

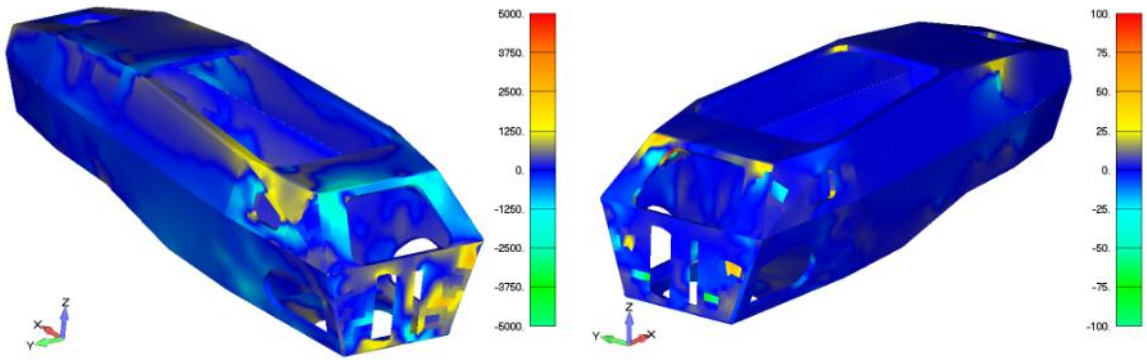

FIGURE 36: CORNER EXIT PRINCIPAL AND SHEAR STRESS

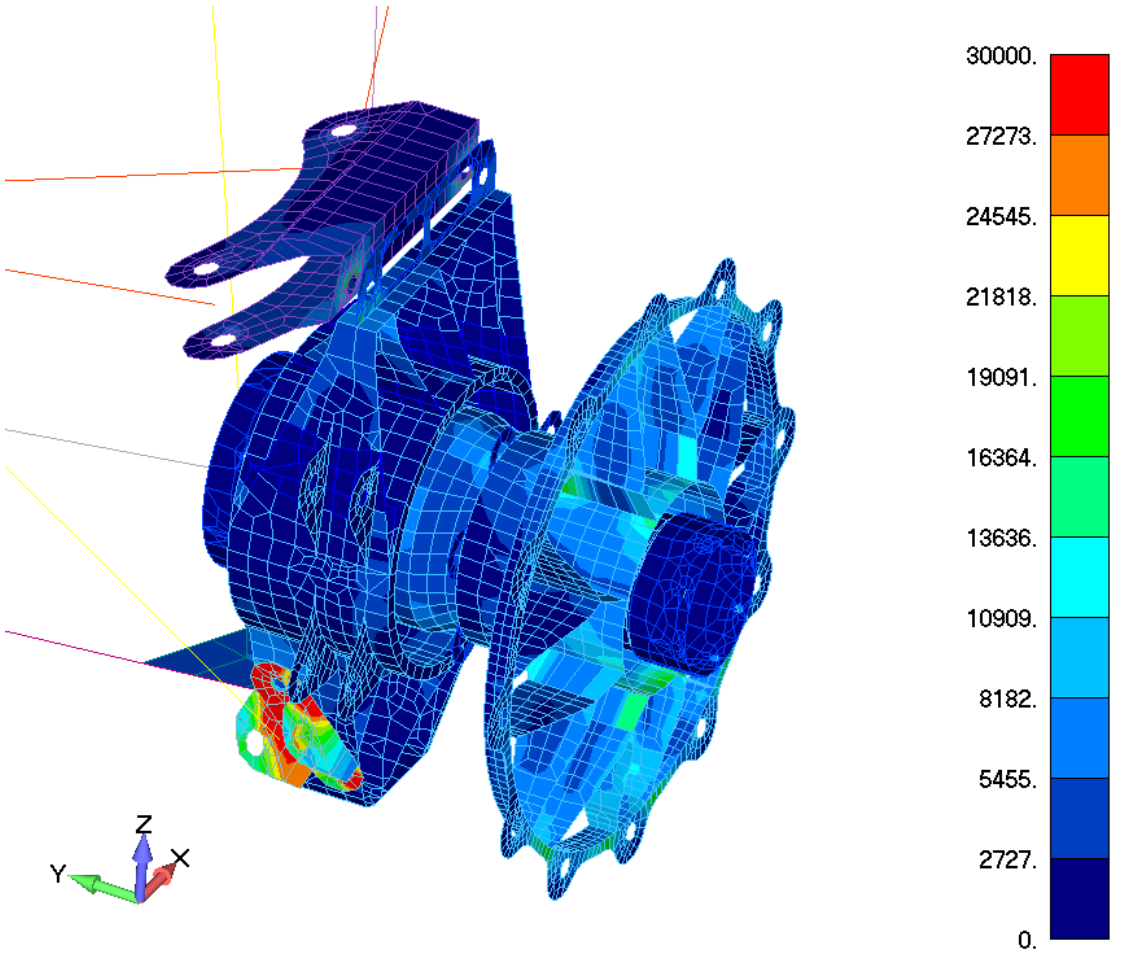

FIGURE 37: CORNER EXIT VON MISES STRESS

5.2.1.5 Bump Results and Discussion

This load case represents the maximum expected design bump load. This drives a significant portion of the vehicle, especially around the shock clevises, as would be expected. What is interesting is that this also drives laminate stress in the bottom of the chassis. This makes sense when one thinks about the whole chassis bending, between the clevis reactions.

	Force (lbf)
Shock	842
FUF	185
FUR	38
FLF	388
FLR	332
Tie Rod	79

TABLE 44: FR BUMP RESULTS

	Force (lbf)
Shock	374
RUF	12
RUR	322
RLF	197
RLR	776
Toe Link	162

TABLE 45: RR BUMP RESULTS

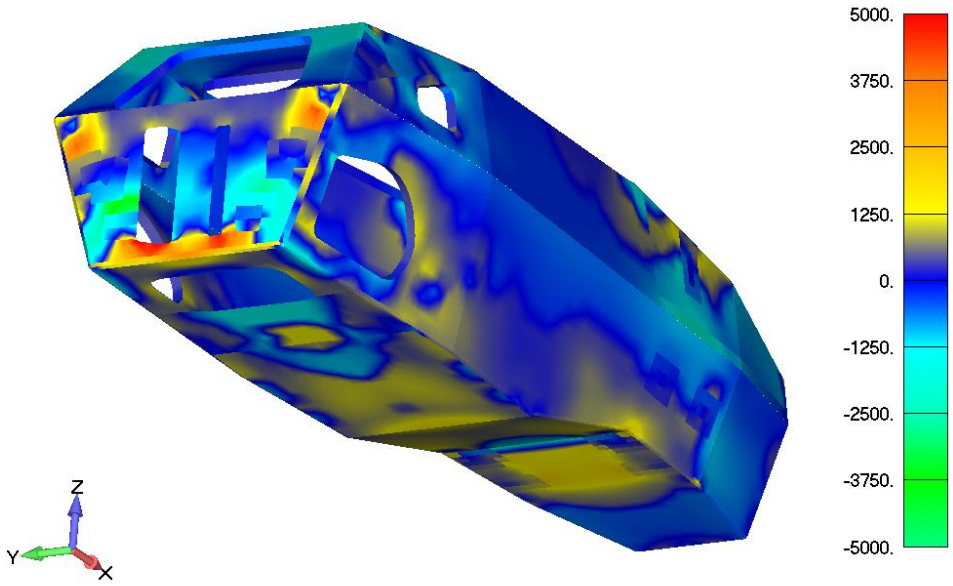

FIGURE 38: BUMP PRINCIPAL STRESS

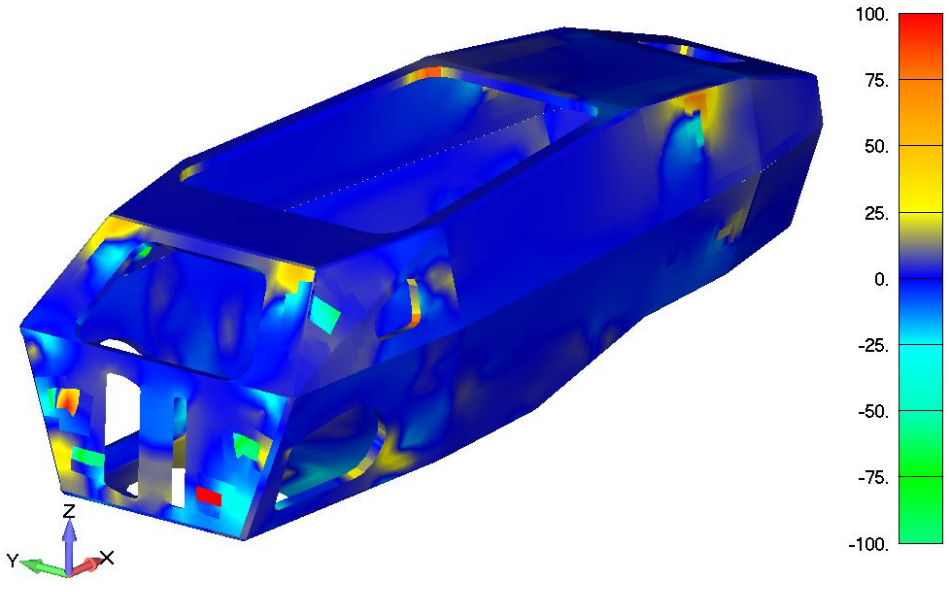

FIGURE 39: BUMP SHEAR STRESS

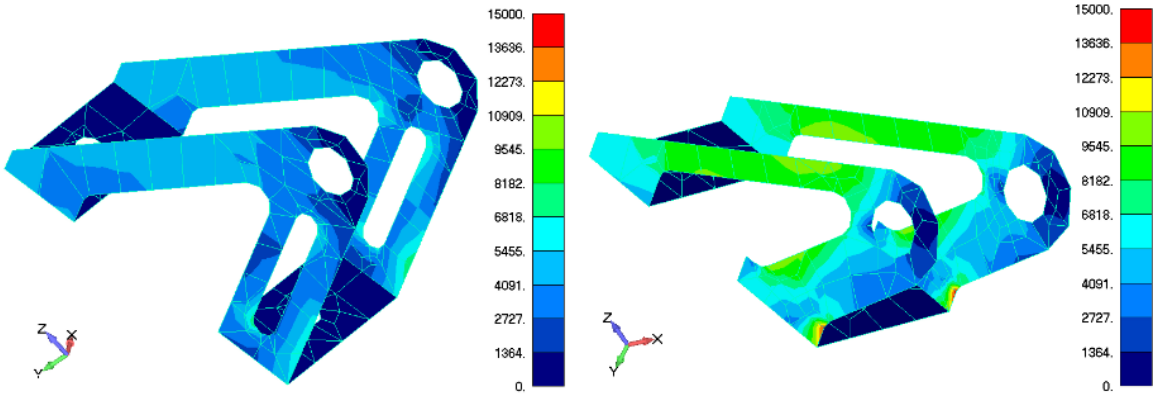

FIGURE 40: BUMP VON MISES STRESS

5.2.1.6 Braking Results and Discussion

This load case represents the maximum straight line braking force. This case notably drives all the front suspension link forces, and the majority of the laminate area around those components. It makes sense that nothing in the rear of the vehicle is affected by this load case, as weight transfer means there is very little normal force or tractive braking force available at the rear tires.

	Force (lbf)
Shock	311
FUF	759
FUR	760
FLF	2648
FLR	2964
Tie Rod	345

TABLE 46: FR BRAKING RESULTS

	Force (lbf)
Shock	38
RUF	34
RUR	22
RLF	10
RLR	83
Toe Link	49

TABLE 47: RR BRAKING RESULTS

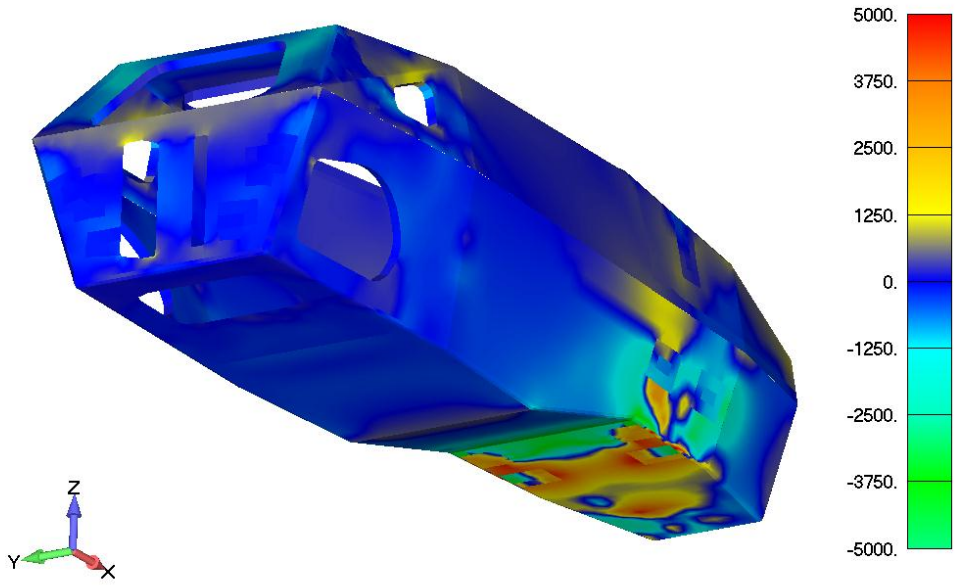

FIGURE 41: BRAKING PRINCIPAL STRESS

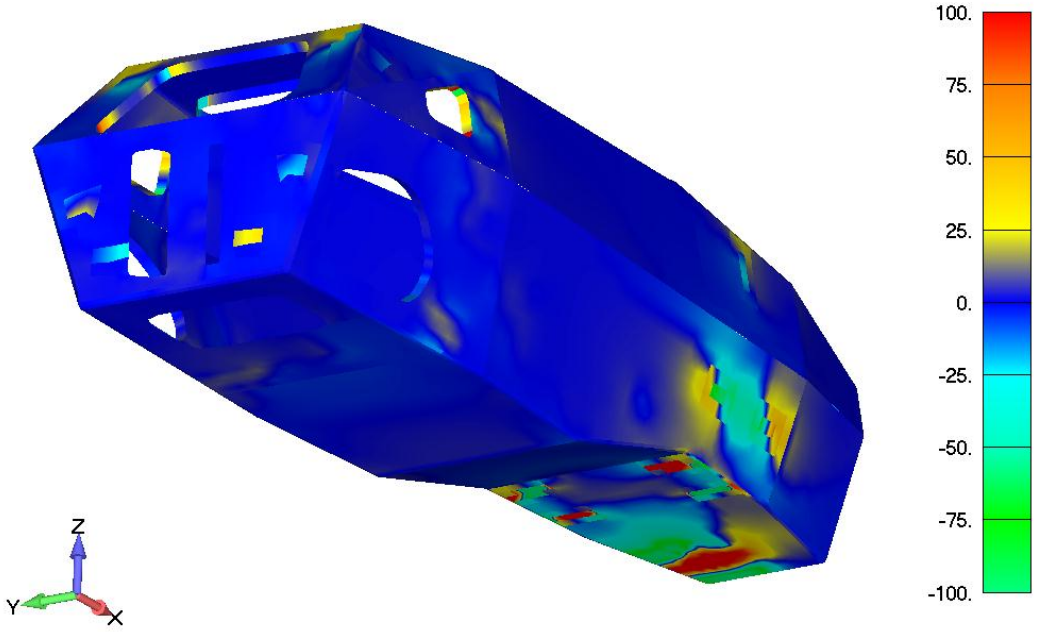

FIGURE 42: BRAKING SHEAR STRESS

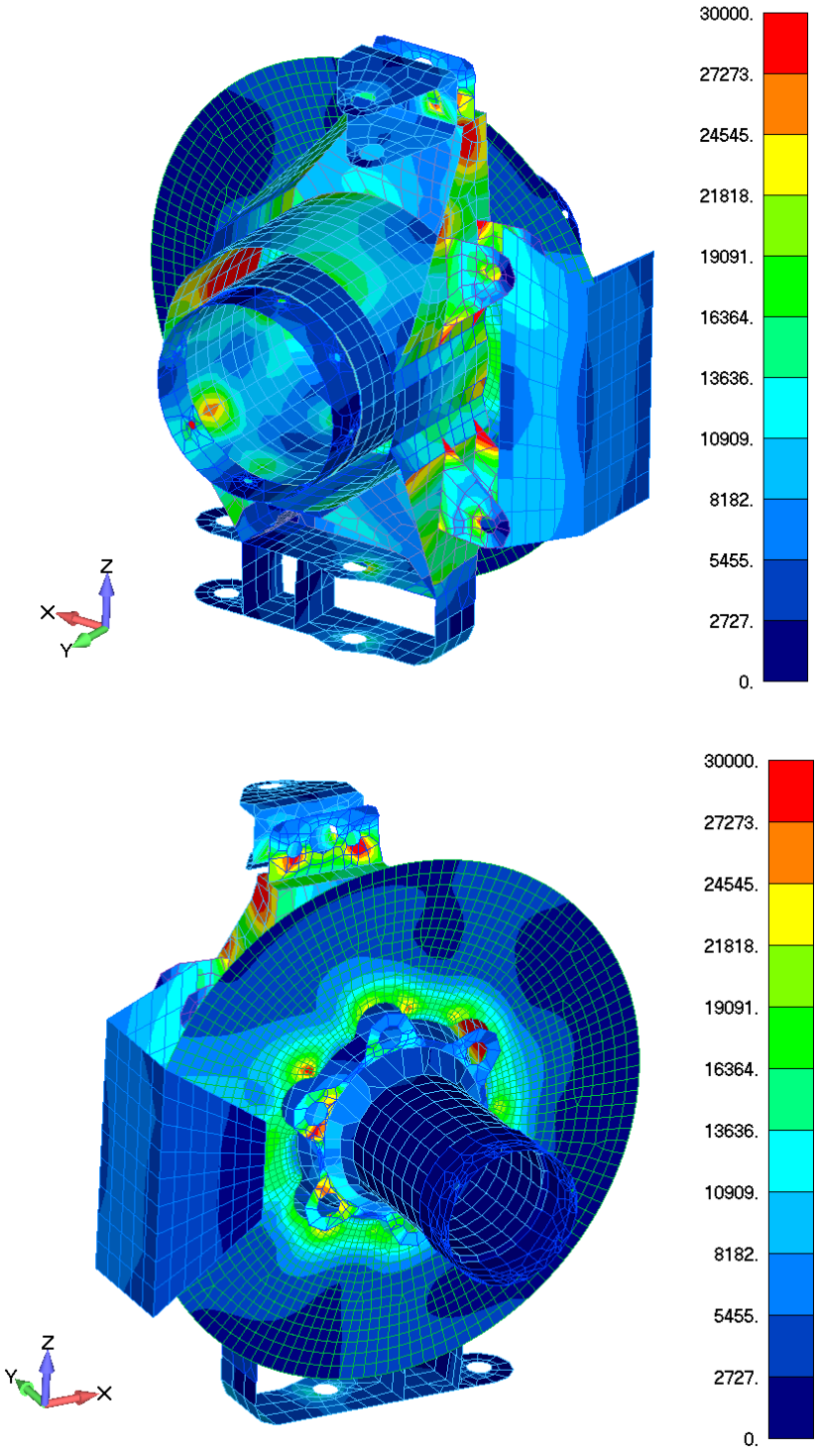

FIGURE 43: BRAKING VON MISES STRESS

5.2.2 Static Test Results

Following are the results of the chassis torsional, toe, and camber stiffness analysis. The chassis and camber stiffness show good agreement to physical tests. The overall hub to hub stiffness does not show good agreement with testing. The installed stiffness show significant deviation from testing. What is interesting is that the chassis stiffness is derived directly from the hub to hub stiffness in testing, so one would expect similar error between the two. What may explain this is the significant deviation in installation stiffness. This could come from either a modeling error or incorrect properties used in the analysis, or poor test data. The test data is sensitive to the data collection method, so this could be a reasonable explanation. This could be shown with repeated testing. The steering toe stiffness also shows significant deviation from physical tests, while the toe stiffness in the rear of the vehicle shows reasonable agreement. This is most easily explained by a modeling deficiency, with a poorly placed RBE2 element that converts a C-channel clevis to effectively a much more rigid box structure.

	Calculated Values				Avg. Error
	Front	Rear	Total		
Hub to hub	N/A	N/A	1503	ft-lb/deg	40%
Installed	2980	2944	N/A	ft-lb/deg	67%
Chassis	N/A	N/A	4982	ft-lb/deg	11%
Toe	198	175	N/A	ft-lb/deg	136%
Camber	220	264	N/A	ft-lb/deg	21%

Table 48: Static Test Results

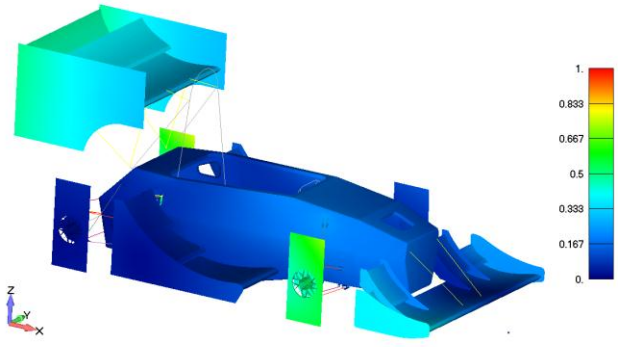

Figure 44: Torsion Test Displacement

5.2.2.1 Torsional Stiffness Results and Discussion

Following are the highest stressed areas for torsional frame and installation stiffness. For installation stiffness, the front right and rear left shock clevises are selected. The Von Mises stress in these components is shown in Figure 45. For torsional frame stiffness, the envelope of all ply principal stresses is shown in Figure 46.

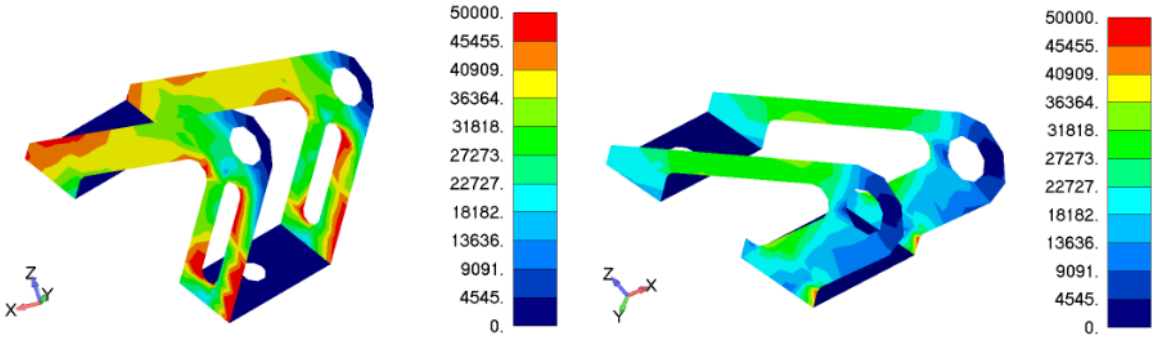

FIGURE 45: TORSION TEST VON MISES STRESS

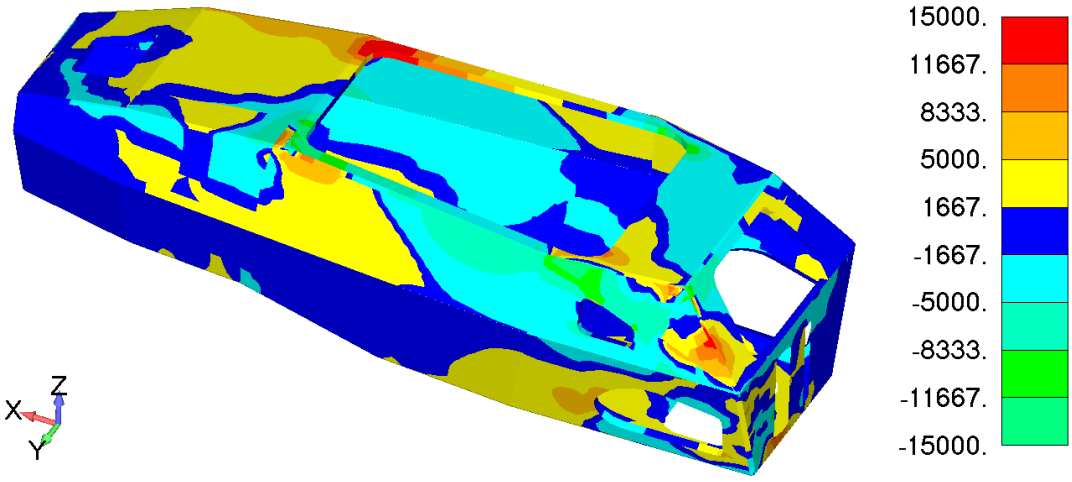

FIGURE 46: TORSION TEST PRINCIPAL STRESS

This load case shows that with the springs replaced by hard links, the load input to the chassis goes directly through these clevises. Due to this specific loading, it appears that the way to improve installation stiffness is by increasing the stiffness of the shock clevis joint and components. Further, the peak stresses in the chassis are not only at the shock

clevis attachment points, but at the corners of the driver opening as well. This shows that the best way to improve chassis torsional stiffness would be to increase either ply modulus, thickness, or core thickness in these areas.

5.2.2.2 Suspension Stiffness Results and Discussion

Following are the highest laminate stress regions for the toe, steering, and camber stiffness tests. For all cases, the envelope of principal stress is shown for the region affected.

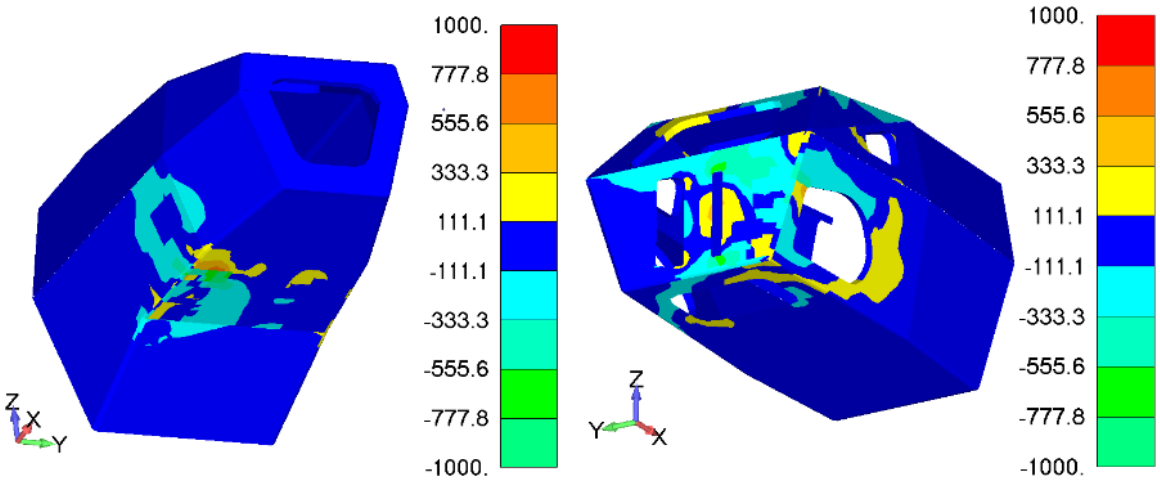

FIGURE 47: STEERING AND TOE STIFFNESS PRINCIPAL STRESS

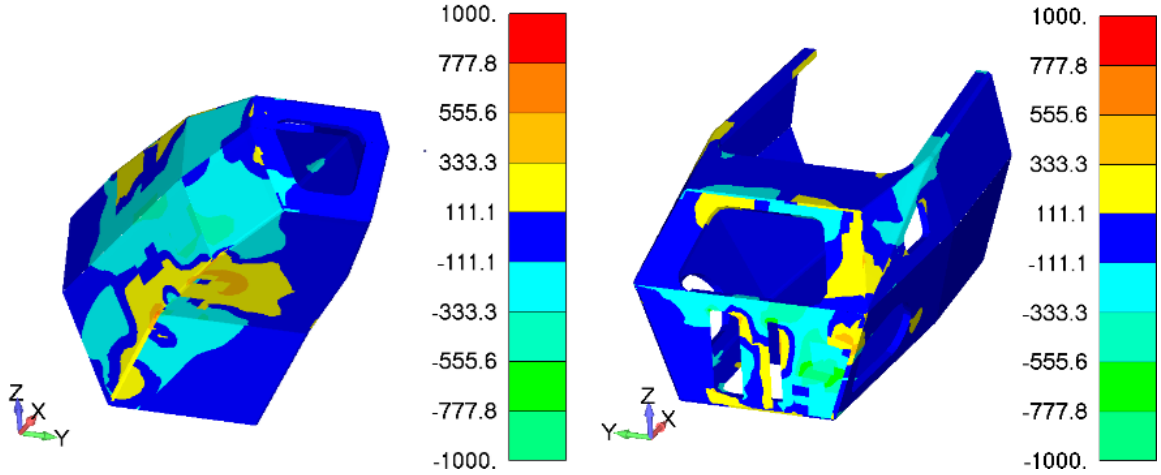

FIGURE 48: CAMBER STIFFNESS PRINCIPAL STRESS

These stiffness tests show the areas of the chassis that are most affected by the different load tests. For steering stiffness, it appears that the front lower front suspension clevis is most affected, although it seems that if the load was reversed a similar result would be found for the front lower rear mount. For toe stiffness, it appears the front suspension clevises and rear chassis opening are most critical. For the front camber test, it appears that the interaction between the upper and lower suspension mounts results in a stress concentration, which could be addressed to increase stiffness in this area. In the rear, it again appears that the rear chassis opening is contributing to the stiffness in this region. Additionally, it seems that the upper engine opening contributes as well. This makes sense, as this test flexes this area nearly directly, and results in 'lozenging' of the opening.

6 CONCLUSION

This work has presented a method for vehicle structural analysis, such that the loads and boundary conditions come from high-level performance requirements. This allows better understanding of the load paths involved in the structure, and the driving load regimes for individual vehicle components. This is of high importance for a performance driven vehicle such as the Formula SAE race car presented here, but it is certainly important to any engineered structure subject to different loading environments, such as airplanes, rockets, boats, etc.

The sources and methods used to assign material properties were analyzed and discussed. While some are straightforward, such as the use of isotropic materials, others, such as laminate properties require care not only in the value selection (derived from physical data), but in their application as well. Further, a technique for deriving tire element structural properties was presented. While this method accomplishes the goal of quick computing time, the load distribution that results does not closely match the expected values. Further investigation into the material properties used could resolve this, however, the root of the problem likely lies in the fact that there is no load distribution outside of the tire to wheel connection. If that is the case, the path forward is either

design components effected by this load in a breakout model that includes the structural properties of air, or create a simplified internal structure that emulates this effect in the high-level model.

The construction techniques used in the finite element model have been analyzed and discussed. A method for calculating the six degrees of freedom around a bolted connection was presented, with results that were within 1.5% of an industry accepted method. While comparing this result to physical testing would be ideal, it is beyond the scope of this work. The use of 2D elements in place of 3D has also been presented, both for the laminate case and for isotropic materials. The laminate case shows agreement with test results within 4%, while the isotropic case shows agreement to 3D elements within 1%. A technique for modeling large bearing connections in a linear elastic model has been presented. This technique shows to largely deviate from the load distribution that would be expected based on contact analysis. However, when one looks outside these local effects this structure proves to transmit load properly, as evidenced from the acceleration load case and the resultant chain tension from applied wheel loads. A combination of contact and CBUSH techniques whereby the elements pulled in tension are removed from the analysis seems to be required to properly analyze local effect around these connections.

Finally, the overall analysis and modeling approach is validated by performing vehicle stiffness tests. A torsional stiffness test was analyzed, and the results compared to physical test data. While the frame stiffness showed agreement within 11% to physical tests, the hub-to-hub and installed stiffness values showed significant deviation. This is likely due to test process errors, possibly either poor data or a poor test fixture. This should be revised to allow these parameters to be properly measured. Additionally, differences between the designed and manufactured components, or the quality of manufacturing, could contribute to this error. The camber stiffness and rear toe stiffness both show good agreement to physical tests, while the front toe stiffness shows significant deviation of 136%. This is likely due to modeling errors that result in a stiffer structure in analysis than exists in reality. From a system loads analysis perspective, this

is unlikely to have a large effect, as this load case is only analyzed in relation to the test. However, this stiffness value is important for steering feel and driver feedback, so revising the model to be able to accurately design to a stiffness value would be important.

6.1 Future Work

The main purpose of this work is to assist in the structural design and development of a Formula SAE vehicle. Therefore, the primary work that needs to be continued is to update the model as required, and use the results presented in refined breakout models.

6.1.1 Modeling

There are multiple updates, to meshes, general components, and properties, to continue to use the model presented. All 2D meshes should be scrutinized for the shape and position of triangular elements within them, and should be manually updated to remove these as they can cause unrealistic stress distributions [22]. This is especially true with meshes that have been auto-generated.

Each large bearing interface should have a contact study performed, and the appropriate elements should be removed from the analysis. Additionally, as components are updated the contact analysis should be repeated, to check for discrepancies.

There are a few components that are missing from this analysis that should be added. The seatback and appropriate connections to the chassis needs to be added, and the driver/chassis connection RBE3 element needs to be updated to reflect this. Bolted connections at each spherical bearing interface could be calculated and added to the analysis. Further, the driver RBE3 element should be updated for specific configurations, i.e. for the acceleration load case, only connect the seatback and floor. For cornering, only connect to floor and chassis side. This would be useful to properly react the drivers' weight into the chassis.

6.1.2 Non-Linear Effects

This analysis is linear, in that the input loads and load distribution follow from the initially set geometry. This leaves out potentially strong effects from changes in angle at

the tire and suspension components that occurs due to suspension travel, tire stiffness, and spring stiffness.

6.1.3 VALIDATION

Validation of model parameters, specifically the mass distribution, should be performed. The vehicle mass moment of inertia in the I_{xx} direction could be measured using a 'see-saw' type test rig. Using a spring of known stiffness constant, one could calculate the MOI from the oscillation period of the system. Similarly, another see-saw and turntable style test rig could measure the I_{yy} and I_{zz} inertias, respectively.

Model validation of specific load cases should be undertaken. This is not a small task, as it requires strain gage implementation of multiple components, including the chassis, suspension links, and drive shafts. Additionally, relative air speed and vehicle accelerations would need to be monitored. Then, the exact test conditions could be analyzed, and the results compared to physical testing.

BIBLIOGRAPHY

[1] MSC.Software Corporation, "Linear Static Analysis User's Guide," MSC.Software Corporation, Santa Ana, 2004.

[2] P. J. Arscott, "Multi Objective Aerodynamic Design in Formula SAE," Oregon State University, Corvallis, 2016.

[3] B. Riley, "Formula SE Anthropometric Reference Data," SAE International, 2015.

[4] SAE International, "2014 FSAE Rules," SAE International, 2014.

[5] R. Story, "Design of Sandwich Panels for a Formula SAE Monocoque Chassis," Oregon State University, Corvallis, 2014.

[6] T. G. Butler and D. Michel, "Nastran, A Summary of the Functions and Capabilities of the NASA Structural Analysis Computer System," National Aeronautics and Space Administration, Washington, 1971.

[7] MSC Software, MSC/Nastran Reference Manual, MSC, 2005.

[8] L. Liao, "A Study of Inertia Relief Analysis," Denver, 2011.

[9] B. Beigi and M. Anvari, "Automotive Body Fatigue Analysis. Inertia Relief or Transient Dynamics?," Detroit, 1999.

[10] G. Bryer and C. Eccles, "Structural Optimization for Vehicle Dynamics Loadcases," vol. 4, no. 1, 2011.

[11] V. Bheemreddy and A. Jensen, "Composite Laminate Modeling," Predictive Engineering, Inc, Portland, 2014.

[12] Predictive Engineering, "Engineering Mechanics White Paper," Predictive Engineering, Inc., Portland, 2013.

[13] W. B. Riley and A. R. George, "Design, Analysis and Testing of a Formula SAE Car Chassis," in *Motorsports Engineering Conference and Exhibition*, Indianapolis, 2002.

[14] H. Huth, "Influence of Fastener Flexibility on the Prediction of Load Transfer and Fatigue Life for Multiple-Row Joints," *Fatigue in Mechanically Fastened Composite and Metallic Joints,* 1986.

[15] Federal Aviation Administration, "Metallic Materials Properties Development and Standardization," National Techical Information Service, Springfield, 2003.

[16] A. Jensen, "Linear Contact Analysis Demystified," Predictive Engineering, Inc., Portland, 2010.

[17] S. K. Clark, Mechanics of Pneumatic Tires, Ann Arbor: National Bureau of Standards, 1971.

[18] Hexcel Corporation, "HexWeb Honeycomb Attributes and Properties," Hexcel, Pleasanton, 1999.

[19] Toray Composites (America), Inc, "Agate Laminate Material Qualification," Toray Composites (America), Inc, 2002.

[20] C. M. S. D. A. B. Kevin H. Brown, "Guideline for Bolted Joint Design and Analysis," Sandia National Laboratories, Albuquerque, 2008.

[21] Predictive Engineering, "Bolt Preload Theory and Application," Predictive Engineering, Inc., Portland, 2011.

[22] R. G. Budynas and J. K. Nisbett, Shigley's Mechanical Engineering Design, New York: McGraw Hill, 2011.

[23] Siemens, "Element Library Reference," Siemens PLM Software, Plano, 2014.

[24] Siemens, "NX Nastran User's Guide," Siemens PLM Software, Plano, 2014.

[25] Goddard Space Flight Center, "Flight Loads Analysis as a Spacecraft Design Tool," Goddard Space Flight Center, 1999.

[26] Marshall Space Flight Center, "Design and Manufacturing Guideline for Aerospace Composites," Marshall Space Flight Center, 1999.

[27] SAE International, "Competition Documents," 2014.

[28] W. F. Milliken and D. L. Milliken, Race Car Vehicle Dynamics, Warrendale: Society of Automotive Engineers, 1995.

[29] Y.-L. Lee, M. E. Barkey and H.-T. Kang, Metal Fatigue Analysis Handbook, San Francisco: Butterworth-Heinemann, 2011.

APPENDICES

APPENDIX A ELEMENT COORDINATE SYSTEMS [23]

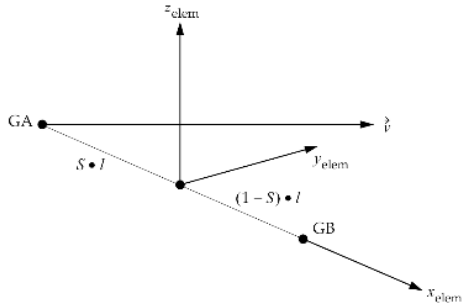

Figure 11-18. CBUSH Element

FIGURE 49: CBUSH COORDINATE SYSTEM

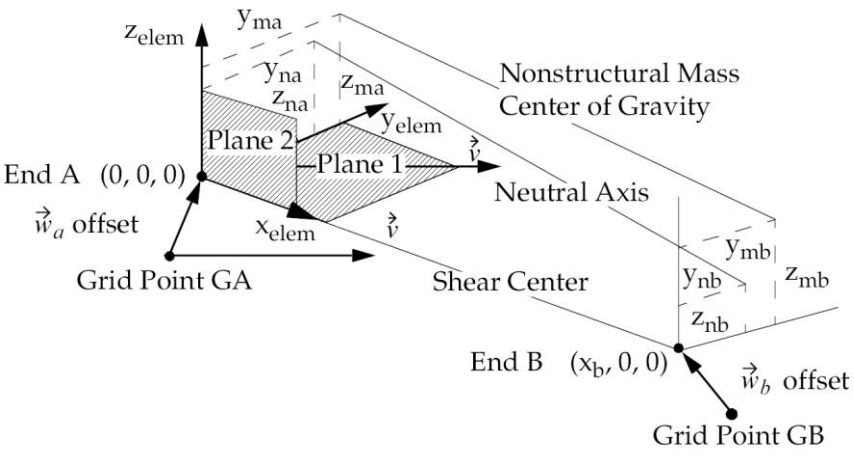

FIGURE 50: CBEAM COORDINATE SYSTEM

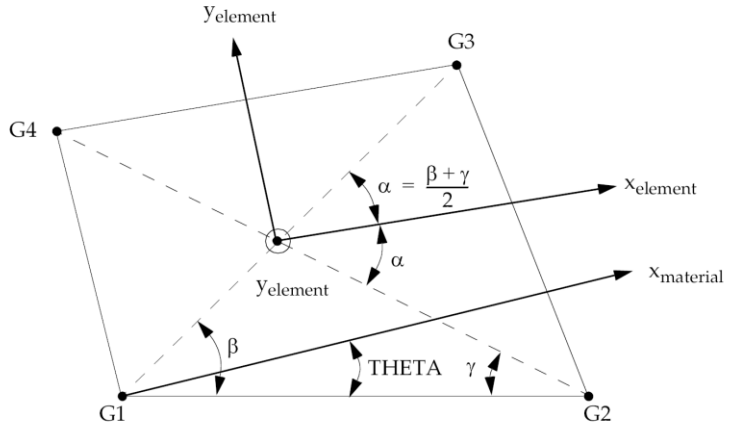

FIGURE 51: CQUAD4 COORDINATE SYSTEM

APPENDIX B ELEMENT ENTRY FORMATS [24]

1	2	3	4	5	6	7	8	9	10
CONM2	EID	G	CID	M	X1	X2	X3		
	I11	I21	I22	I31	I32	I33			

FIGURE 52: MASS ELEMENT BULK ENTRY

1	2	3	4	5	6	7	8	9	10
CBUSH	EID	PID	GA	GB	GO/X1	X2	X3	CID	
	S	OCID	S1	S2	S3				

FIGURE 53: CBUSH BULK ENTRY

1	2	3	4	5	6	7	8	9	10
CBEAM	EID	PID	GA	GB	X1	X2	X3	BIT	
	PA	PB	W1A	W2A	W3A	W1B	W2B	W3B	
	SA	SB							

FIGURE 54: CBEAM BULK ENTRY

1	2	3	4	5	6	7	8	9	10
CQUAD4	EID	PID	G1	G2	G3	G4	THETA or MCID	ZOFFS	
		TFLAG	T1	T2	T3	T4			

FIGURE 55: SHELL BULK ENTRY

1	2	3	4	5	6	7	8	9	10
RBE2	EID	GN	CM	GM1	GM2	GM3	GM4	GM5	
	GM6	GM7	GM8	-etc.-	ALPHA				

FIGURE 56: RBE2 BULK ENTRY

1	2	3	4	5	6	7	8	9	10
RBE3	EID		REFGRID	REFC	WT1	C1	G1,1	G1,2	
	G1,3	WT2	C2	G2,1	G2,2	-etc.-	WT3	C3	
	G3,1	G3,2	-etc.-	WT4	C4	G4,1	G4,2	-etc.-	
	"UM"	GM1	CM1	GM2	CM2	GM3	CM3		
		GM4	CM4	GM5	CM5	-etc.-			
	"ALPHA"	ALPHA							

FIGURE 57: RBE3 BULK ENTRY

APPENDIX C ELEMENT PROPERTY CARDS

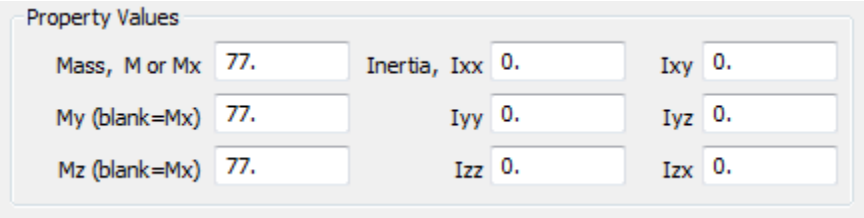

FIGURE 58: MASS PROPERTY CARD

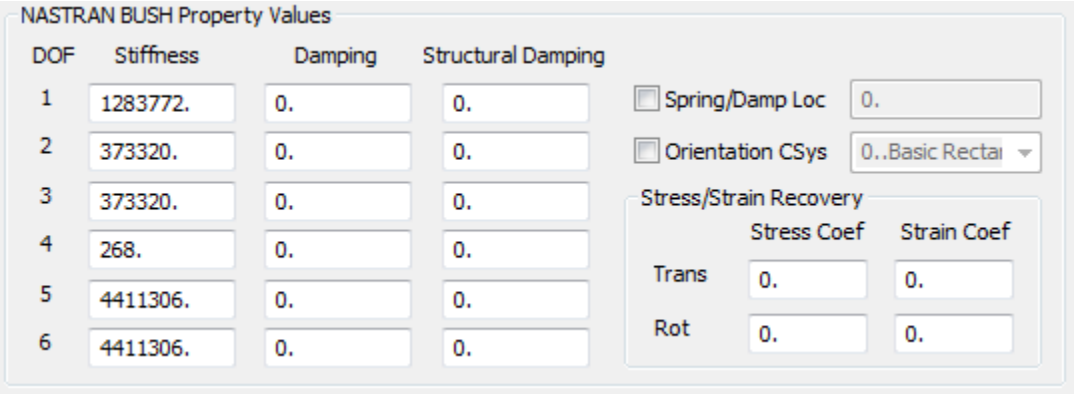

FIGURE 59: CBUSH PROPERTY CARD

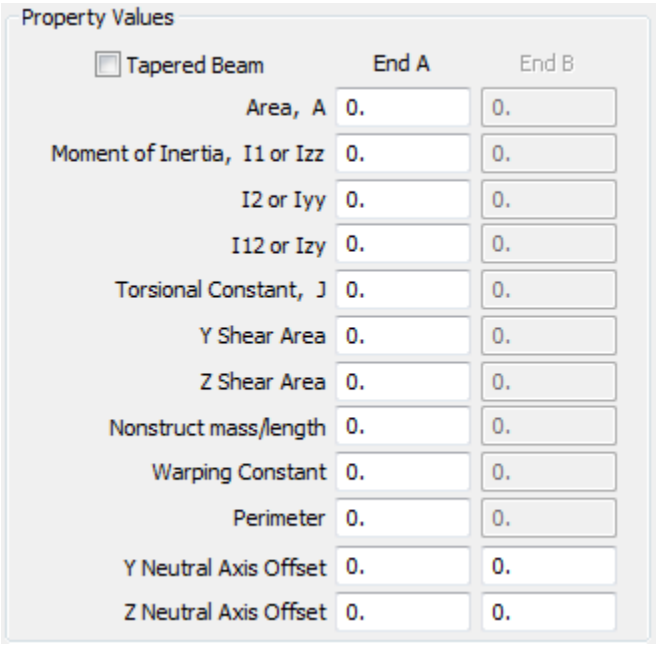

FIGURE 60: CBEAM PROPERTY CARD

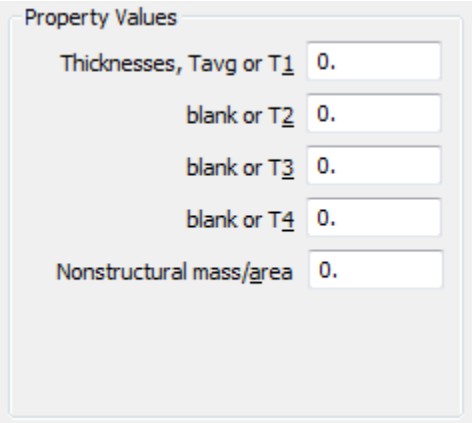

FIGURE 61: PLATE PROPERTY CARD

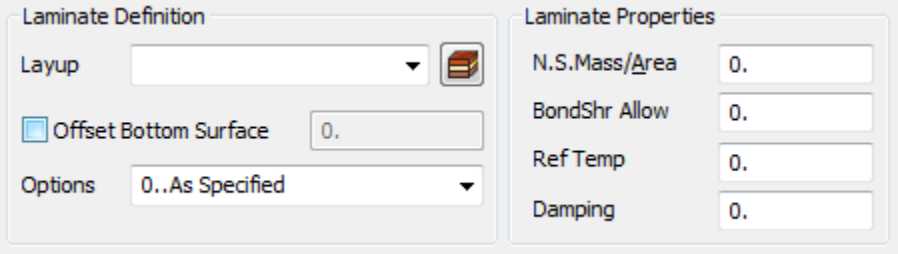

FIGURE 62: LAMINATE PROPERTY CARD

--- Top of Layup --- Total Thickness = 0.638

Ply ID	Global Ply	Material	Thickness	Angle
11		3..T700-2510 Plain Weave	0.015	45.
10		5..M46J-2510 Uni	0.009	0.
9		3..T700-2510 Plain Weave	0.015	0.
8		3..T700-2510 Plain Weave	0.015	0.
7		3..T700-2510 Plain Weave	0.015	45.
6		4..Hexcel HRH-10-1/8-3/0	0.5	0.
5		3..T700-2510 Plain Weave	0.015	45.
4		3..T700-2510 Plain Weave	0.015	0.
3		3..T700-2510 Plain Weave	0.015	0.
2		5..M46J-2510 Uni	0.009	0.
1		3..T700-2510 Plain Weave	0.015	45.

--- Bottom of Layup ---

FIGURE 63: LAYUP DEFINITION

APPENDIX D MOMENT OF INERTIA APPROXIMATION

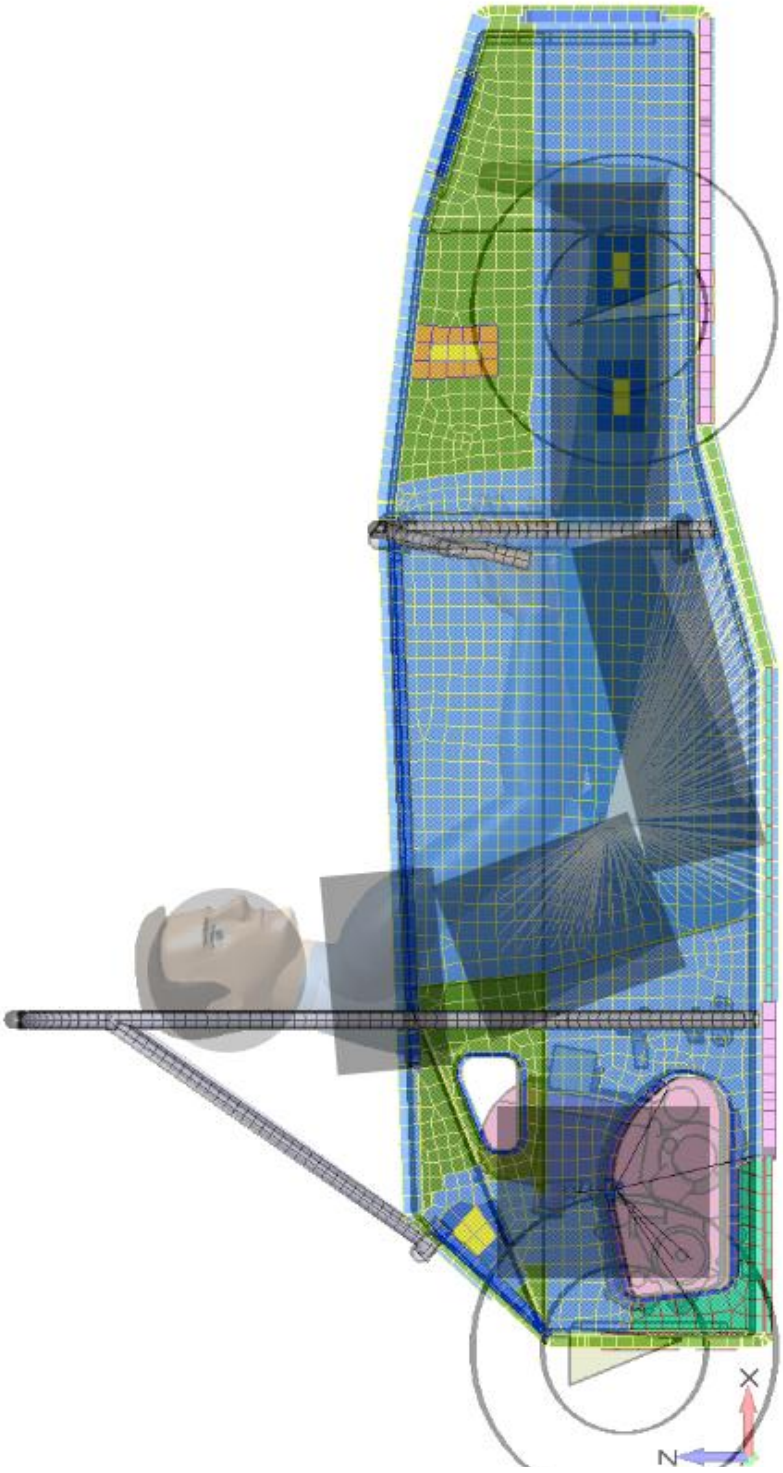

FIGURE 64: MASS MOI REPRESENTATION

APPENDIX E TIRE VERTICAL LOAD TEST AND SIMULATION

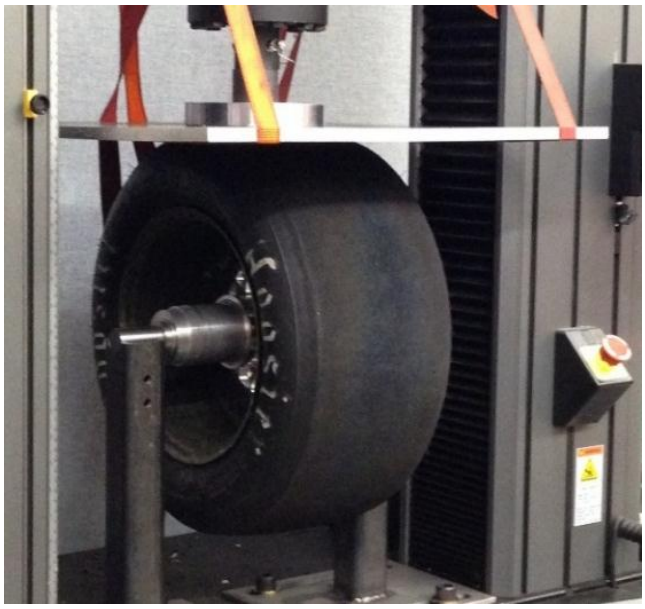

FIGURE 65: PHYSICAL TIRE TEST

	Series Name	Pressure (psi)	Max Load (lb)	Extension (in)
1	GFR2017.WH.02.01	22	900	0.91
2	GFR2017.WH.02.02	20.3	900	0.93
3	GFR2017.WH.02.03	18.85	900	0.97
4	GFR2017.WH.02.04	17.4	900	1.04
5	GFR2017.WH.02.05	15.95	900	1.08
6	GFR2017.WH.02.06	14.5	900	1.17
7	GFR2017.WH.02.07	13.05	900	1.25
8	GFR2017.WH.02.08	11.6	900	1.35
9	GFR2017.WH.02.09	10.15	900	1.44
10	GFR2017.WH.02.10	8.7	900	1.62

TABLE 49: PHYSICAL TIRE TEST DATA

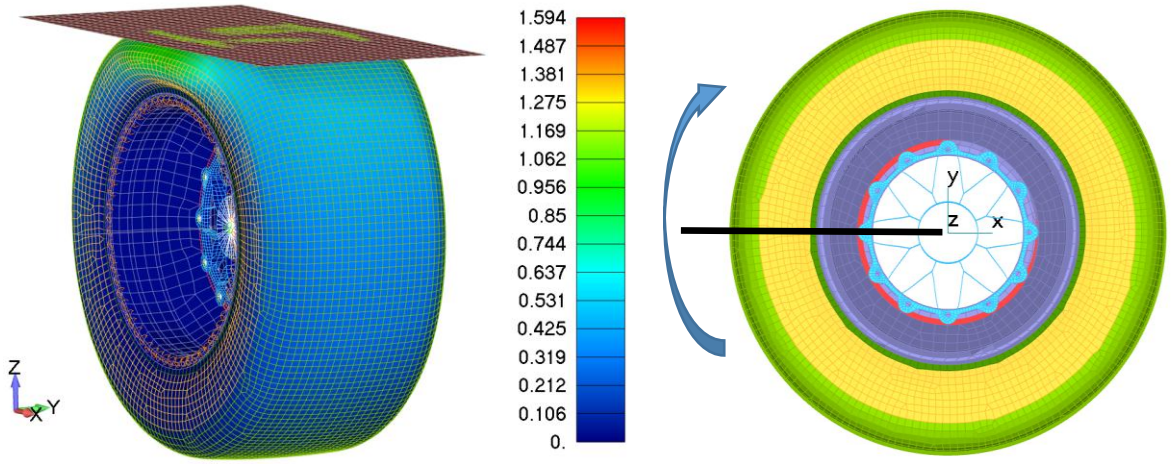

FIGURE 66: TIRE TEST SIMULATION, 8.7PSI

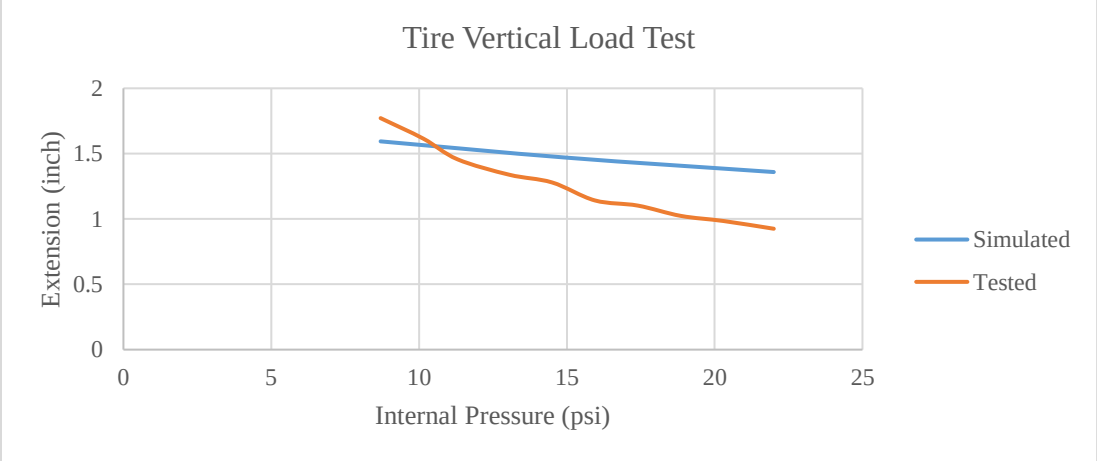

FIGURE 67: TIRE TEST COMPARISON

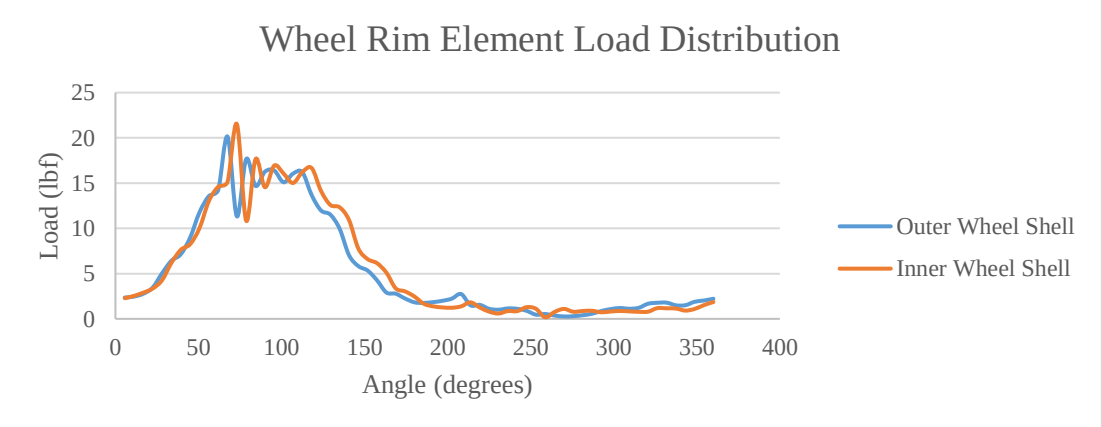

FIGURE 68: SIMULATED RIM CONNECTION FORCES

APPENDIX F SANDWICH PANEL TEST DATA

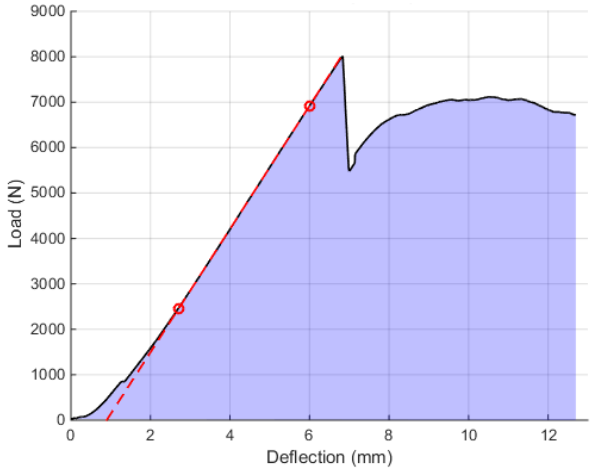

FIGURE 69: 3 POINT BEND PHYSICAL TEST

--- Top of Layup --- Total Thickness = 1.114

Ply ID	Global Ply	Material	Thickness	Angle
9		3..T700-2510 Plain Weave	0.015	45.
8		13..M40J-2510 Plain Weave	0.012	0.
7		3..T700-2510 Plain Weave	0.015	0.
6		3..T700-2510 Plain Weave	0.015	45.
5		4..Hexcel HRH-10-1/8-3/0	1.	0.
4		3..T700-2510 Plain Weave	0.015	0.
3		3..T700-2510 Plain Weave	0.015	0.
2		13..M40J-2510 Plain Weave	0.012	0.
1		3..T700-2510 Plain Weave	0.015	45.

--- Bottom of Layup ---

FIGURE 70: 3 POINT BEND LAYUP SCHEDULE

GFR2015.BB.01 Test Results		
Max Load	8017	N
Deflection at Max Load	6.84	mm
x1	2.7	mm
x2	6	mm
y1	2463	N
y2	6921	N
Test Gradient	1350	N/mm
Adjusted Gradient	1722	N/mm

TABLE 50: 3 POINT BEND TEST DATA

APPENDIX G TIRE LOADS

Static Weight Distribution			
Distribution with 95th percentile driver	FL	118.23	lb
	FR	118.23	lb
	RL	163.27	lb
	RR	163.27	lb
Distribution with 150 lb percentile driver	FL	103.53	lb
	FR	103.53	lb
	RL	142.97	lb
	RR	142.97	lb
Distribution with 5th percentile driver	FL	95.13	lb
	FR	95.13	lb
	RL	131.37	lb
	RR	131.37	lb

TABLE 51: TIRE LOADS, STATIC WEIGHT

Static Weight Distribution + Load Transfer			
Lateral Accel	a	2.5	g
Distribution with 95th percentile driver	FL	-66.5242	lb
	FR	302.9842	lb
	RL	-21.4842	lb
	RR	348.0242	lb
Longitudinal Decel	a	2	g
Distribution with 95th percentile driver	FL	225.2184	lb
	FR	225.2184	lb
	RL	56.2816	lb
	RR	56.2816	lb
Longitudinal Accel	a	1	g
Distribution with 95th percentile driver	FL	64.7358	lb
	FR	64.7358	lb
	RL	216.7642	lb
	RR	216.7642	lb

TABLE 52: TIRE LOADS, STATIC WEIGHT AND LOAD TRANSFER

APPENDIX H CFD PLOTS, 65 KPH

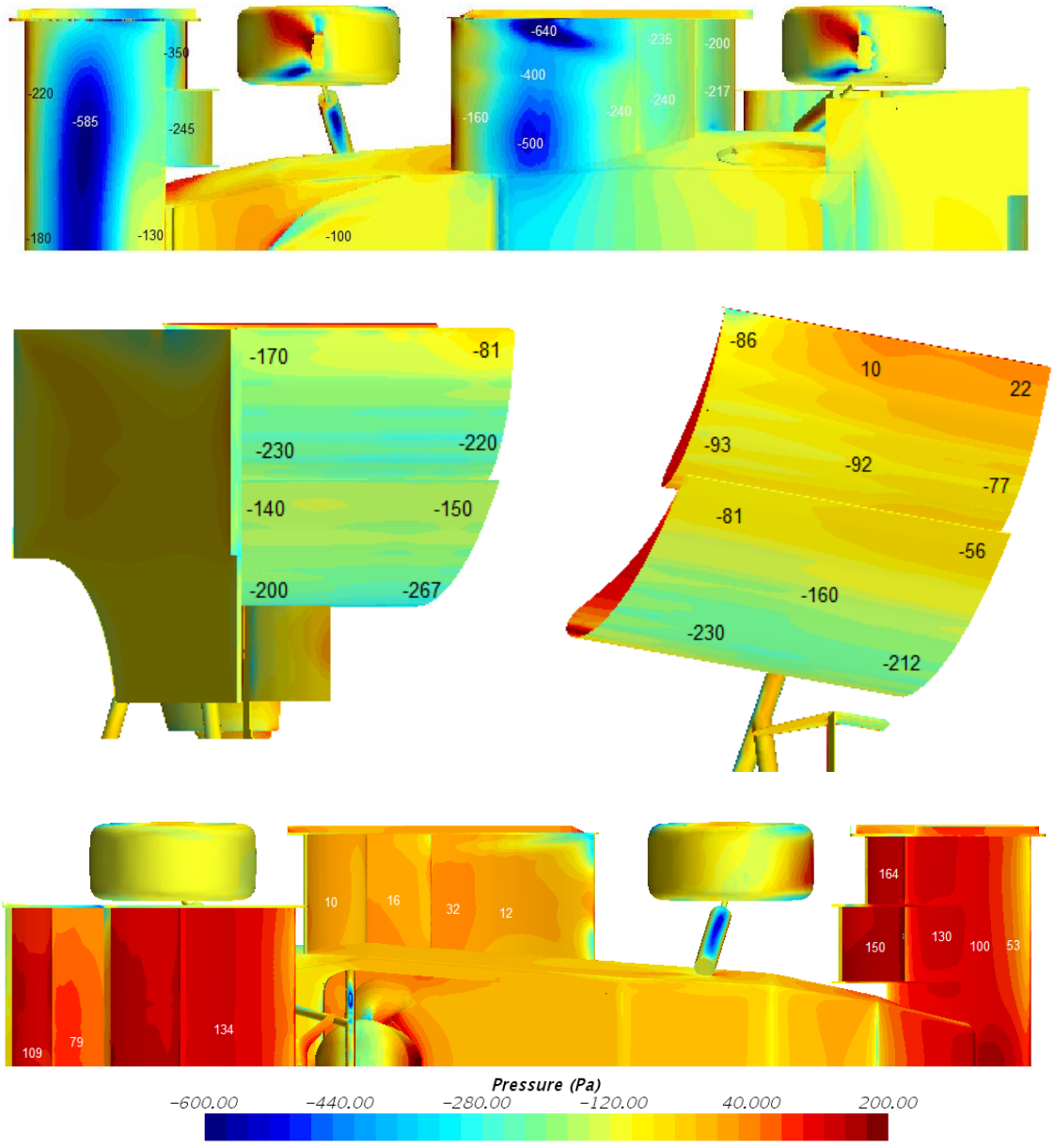

FIGURE 71: CFD PRESSURE PLOTS, 65KPH